Supplement of Atmos. Chem. Phys., 23, 1731–1747, 2023
https://doi.org/10.5194/acp-23-1731-2023-supplement

Atmospheric Chemistry and Physics
Open Access
EGU

Supplement of

Effects of pH and light exposure on the survival of bacteria and their ability to biodegrade organic compounds in clouds: implications for microbial activity in acidic cloud water

Yushuo Liu et al.

Correspondence to: Theodora Nah (theodora.nah@cityu.edu.hk)

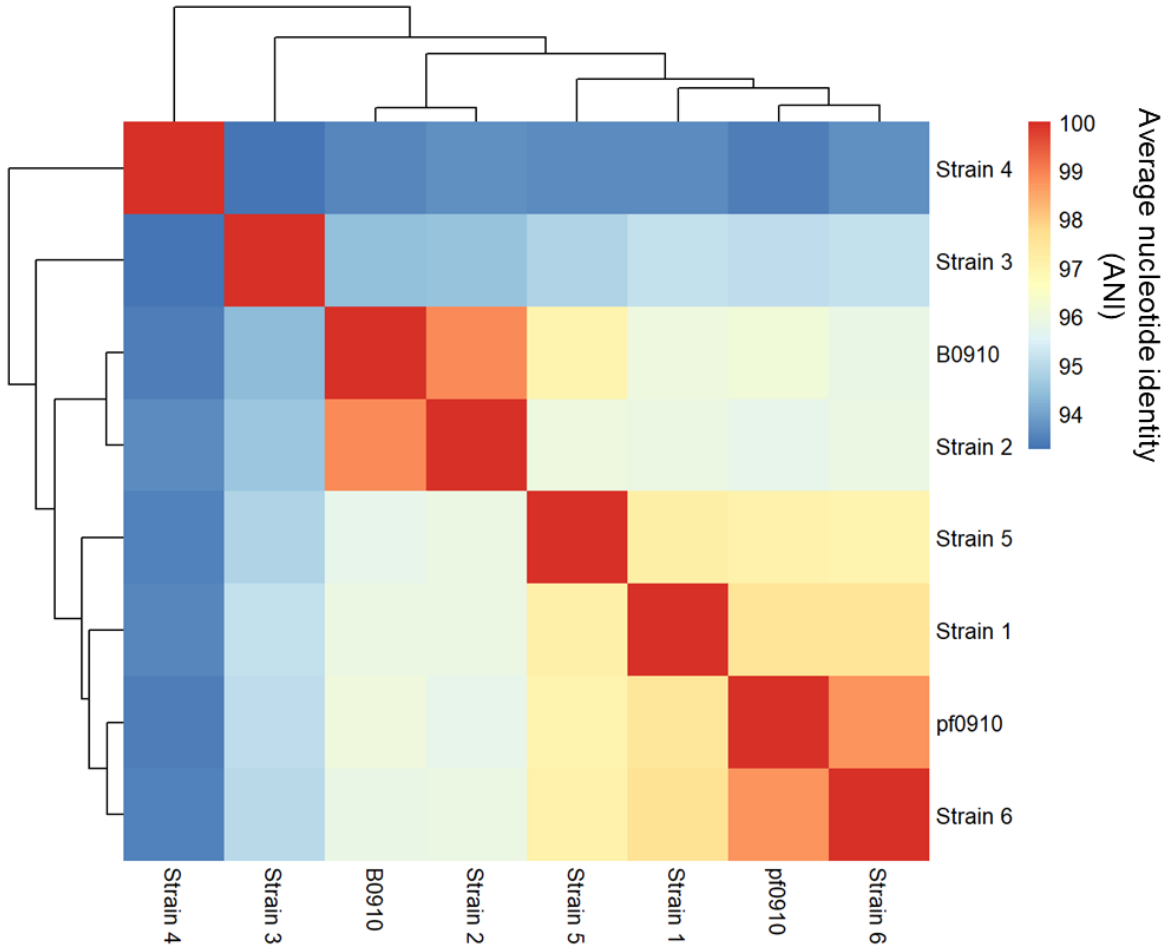

Figure S1. Average nucleotide identity (ANI) value of *Enterobacter* strains B00910, pf0910, and six others. **Strain 1:** *Enterobacter hormaechei* subsp. *oharae* DSM 16687; **Strain 2:** *Enterobacter hormaechei* subsp.hoffmannii DSM 14563; **Strain 3:** *Enterobacter hormaechei* ATCC 49162; **Strain 4**: *Enterobacter quasihormaechei*. GCF 004331385.1; **Strain 5:** *Enterobacter xiangfangensis* LMG27195; **Strain 6:** *Enterobacter hormaechei* subsp. *steigerwaltii* DSM 16691. Strains 1 to 6 are the closest identified neighbors with strains B0910 and pf0910.

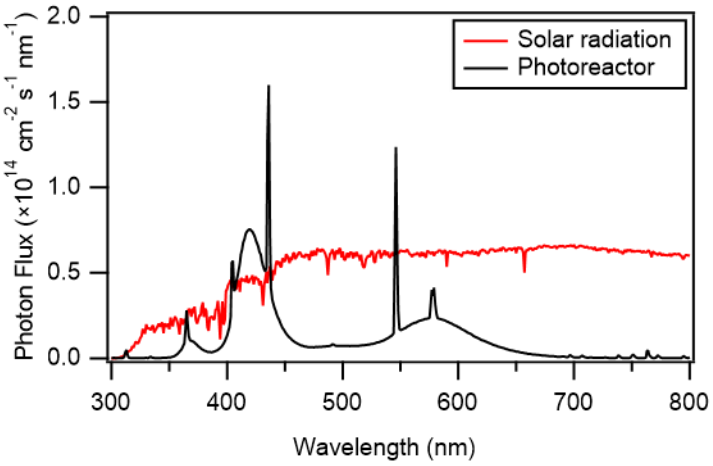

Figure S2. Photon flux inside of the photoreactor (black) and actinic flux for a fall day in Hong Kong in the morning (red). One lamp with output centered at ~365 nm (RPR-3500A, Southern New England Ultraviolet Company), four lamps with outputs centered at ~421 nm (RPR-4190A, Southern New England Ultraviolet Company), and three lamps with outputs centered at ~580 nm (RPR-5750A, Southern New England Ultraviolet Company) were used to illuminate solutions in the photoreactor.

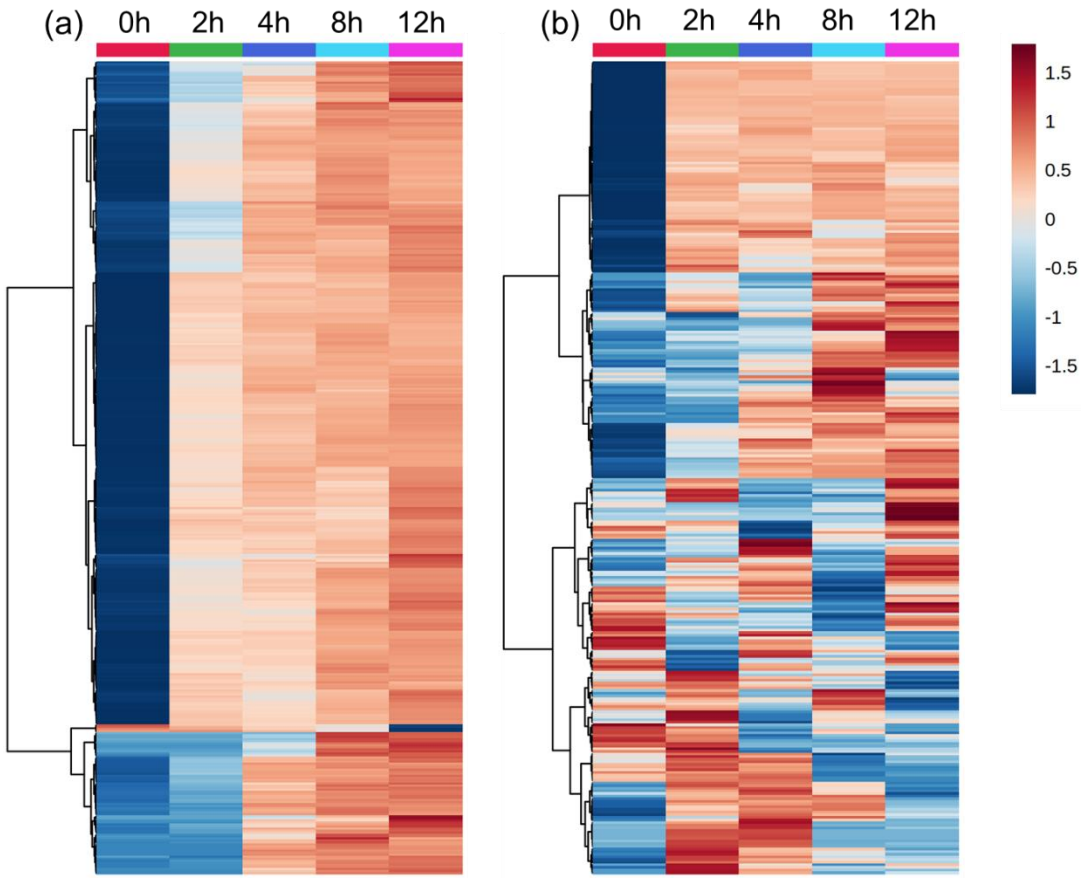

Figure S3. Heat maps showing the time evolution of (a) water-soluble compounds and (b) water-insoluble compounds from *E. hormaechei* B0910 during exposure to simulated sunlight at pH 4.3. The heat maps were generated from non-targeted UPLC-MS analysis of samples with different light exposure times. 259 water-soluble compounds and 215 water-insoluble compounds were selected based on PLS-DA results (VIP > 1.0 criteria). The average UPLC-MS intensity of each compound at each light exposure time was obtained from the nine replicates. The average UPLC-MS intensities were subsequently log10 transformed and auto scaled (i.e., mean-centered and divided by the standard deviation of each variable). The color scale ranges from red color for high abundance to blue for low abundance.

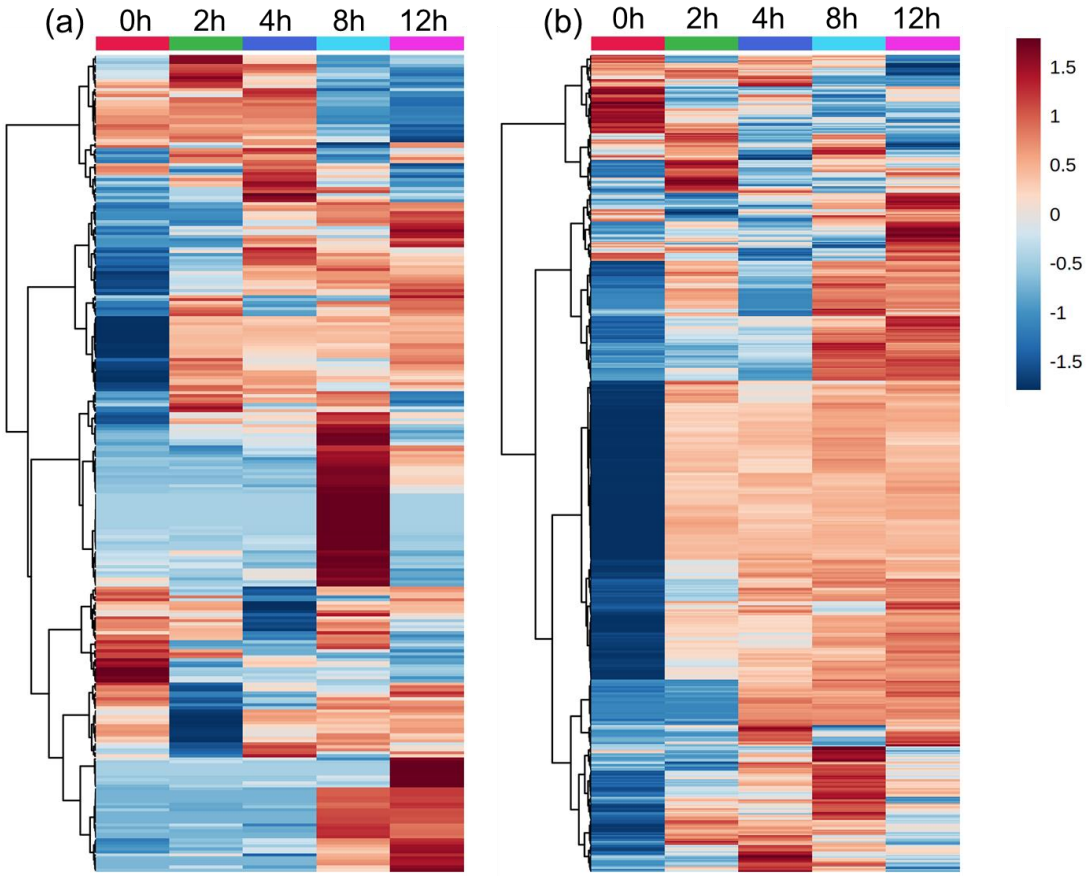

Figure S4. Heat maps showing the time evolution of (a) water-soluble compounds and (b) water-insoluble compounds from *E. hormaechei* pf0910 during exposure to simulated sunlight at pH 4.3. The heat maps were generated from non-targeted UPLC-MS analysis of samples with different light exposure times. 209 water-soluble compounds and 251 water-insoluble compounds were selected based on PLS-DA results (VIP > 1.0 criteria). The average UPLC-MS intensity of each compound at each light exposure time was obtained from the nine replicates. The average UPLC-MS intensities were subsequently log10 transformed and auto scaled (i.e., mean-centered and divided by the standard deviation of each variable). The color scale ranges from red color for high abundance to blue for low abundance.

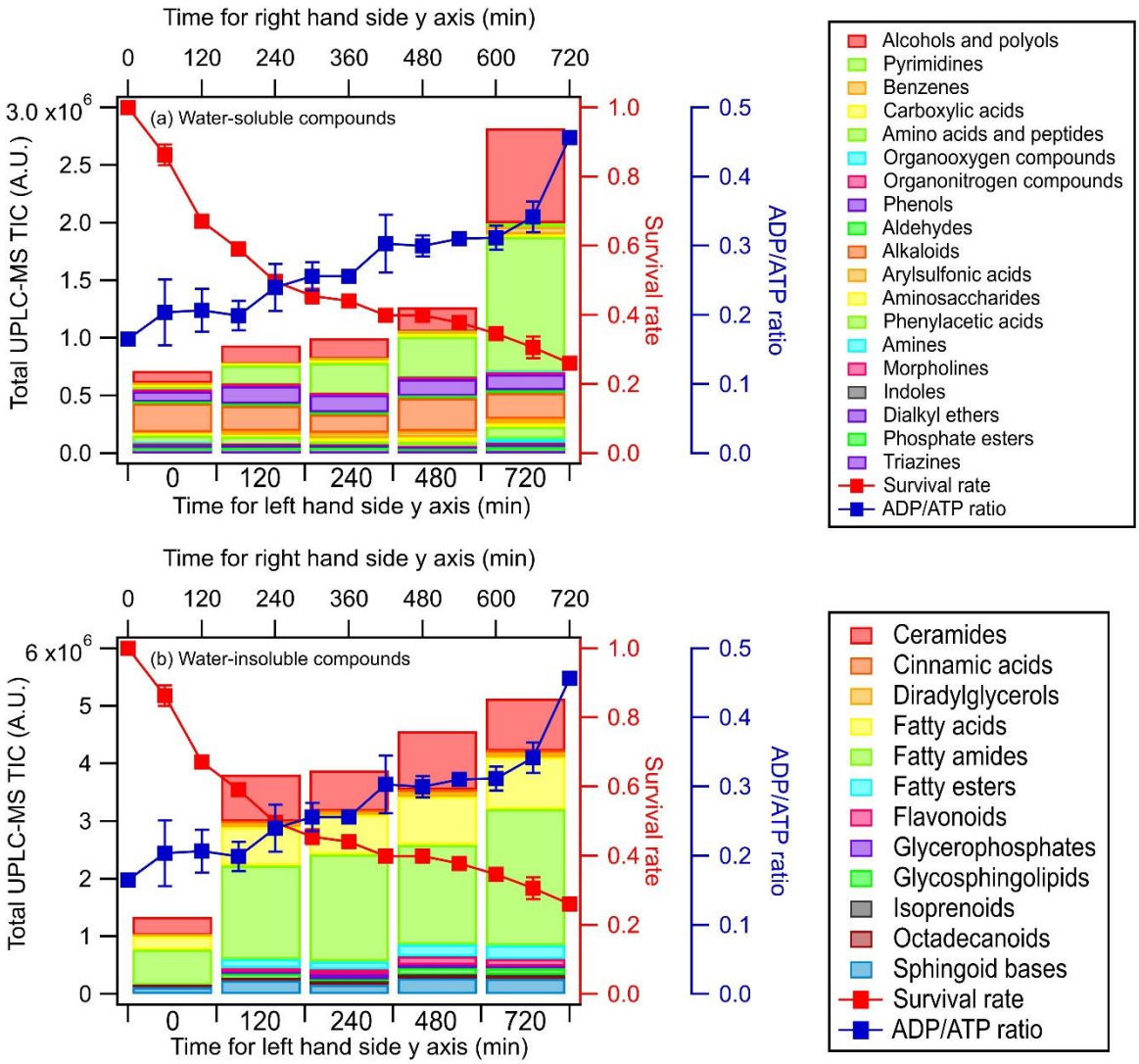

Figure S5. Time evolution of the UPLC-MS total ion chromatograph (TIC) signals of (a) water-soluble compounds, and (b) water-insoluble compounds from *E. hormaechei* pf0910 during exposure to simulated sunlight at pH 4.3 over time. These compounds are classified based on their chemical functionality. Also shown are the time evolution of the survival rate and ADP/ATP ratio of *E. hormaechei* pf0910.

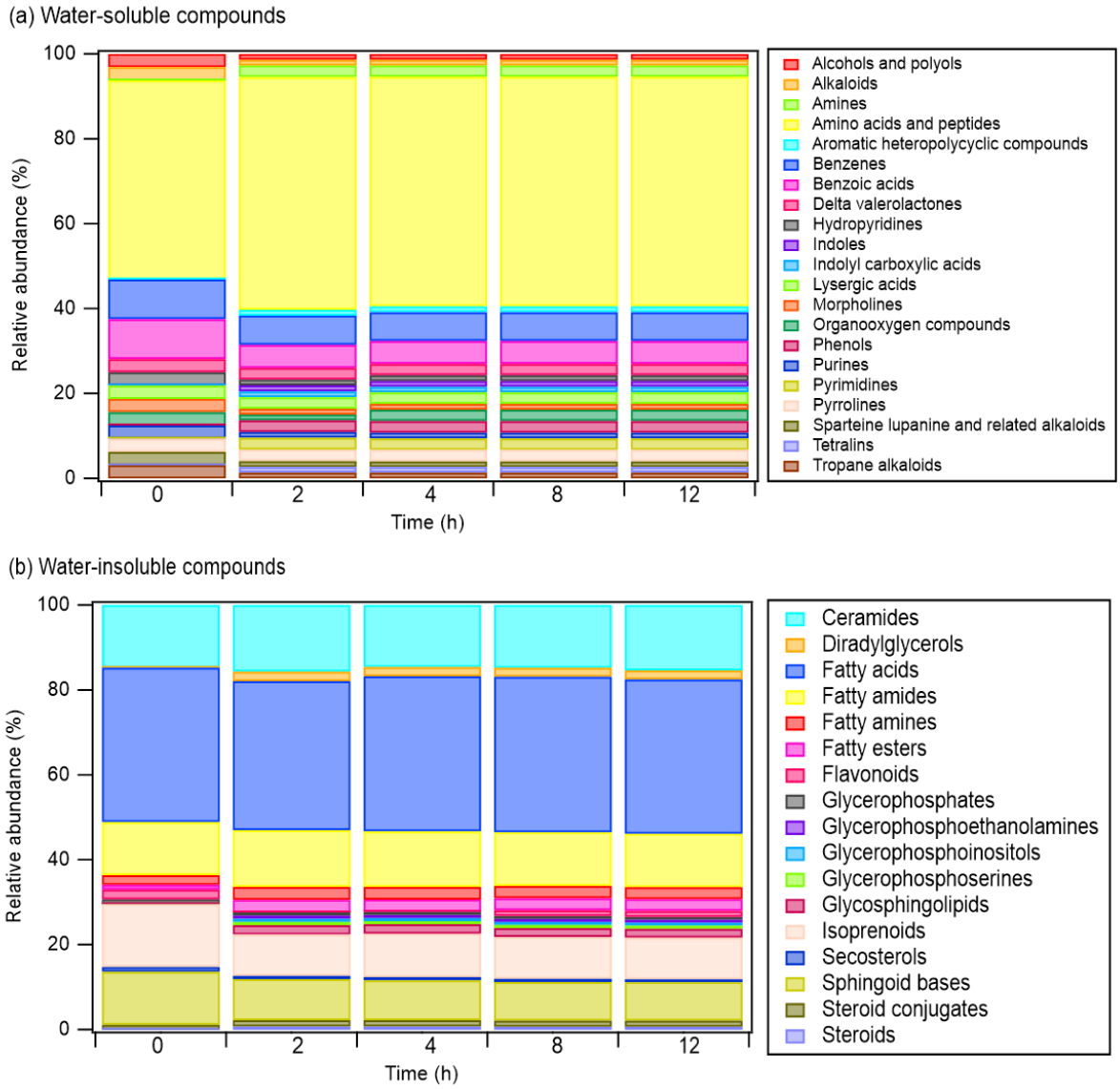

Figure S6. Relative abundance of the different classes of (a) water-soluble compounds, and (b) water-insoluble compounds from *E. hormaechei* B0910 during exposure to simulated sunlight at pH 4.3.

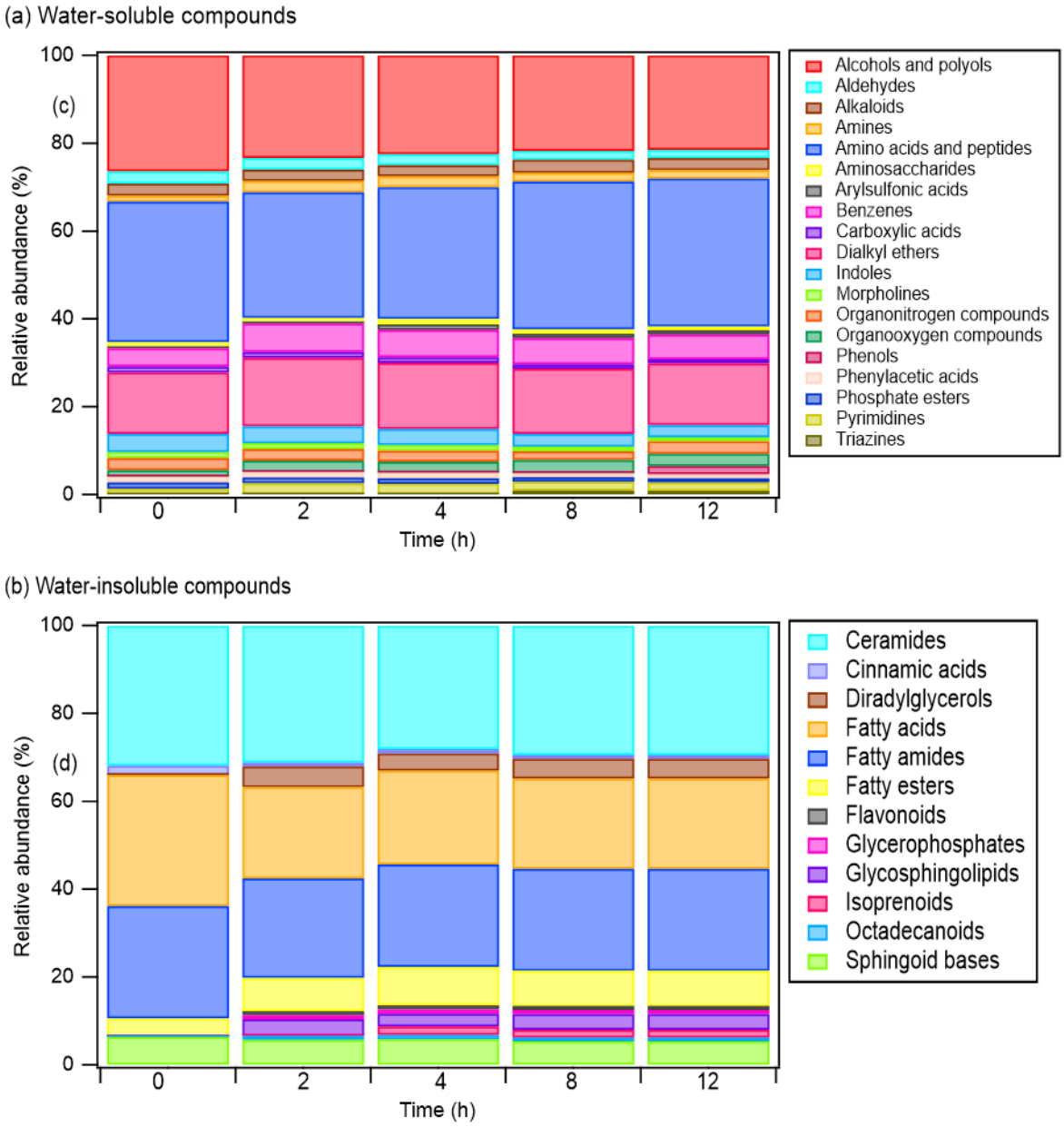

Figure S7. Relative abundance of the different classes of (c) water-soluble compounds, and (d) water-insoluble compounds from *E. hormaechei* pf0910 during exposure to simulated sunlight at pH 4.3.

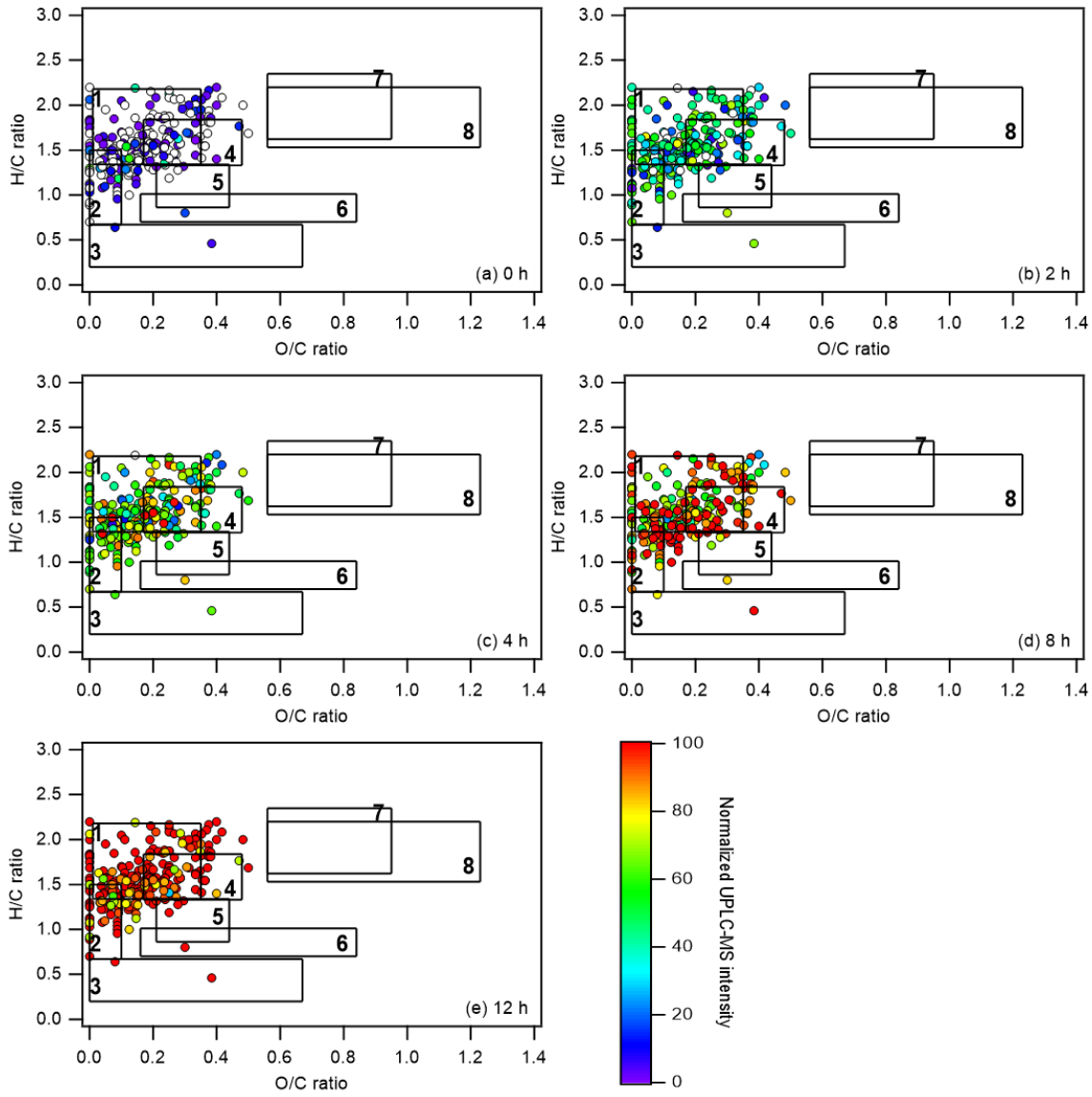

Figure S8. Van Krevelen diagrams of water-soluble compounds from *E. hormaechei* B0910 during exposure to simulated sunlight at pH 4.3 taken at different time points of the experiment: (a) 0 h, (b) 2 h, (c) 4 h, (d) 8 h, and (e) 12 h. The color of each symbol denotes its UPLC-MS intensity at that specific time point normalized to its maximum UPLC-MS intensity obtained during the entire experiment. Symbols that are colored white indicates that these compounds were not detected at that specific time point. The Van Krevelen diagrams are divided into eight chemical classes based on their O/C and H/C ratios: (1) lipids, (2) unsaturated hydrocarbons, (3) condensed aromatic structures, (4) peptides, (5) lignin, (6) tannin, (7) amino sugars, and (8) carbohydrates.

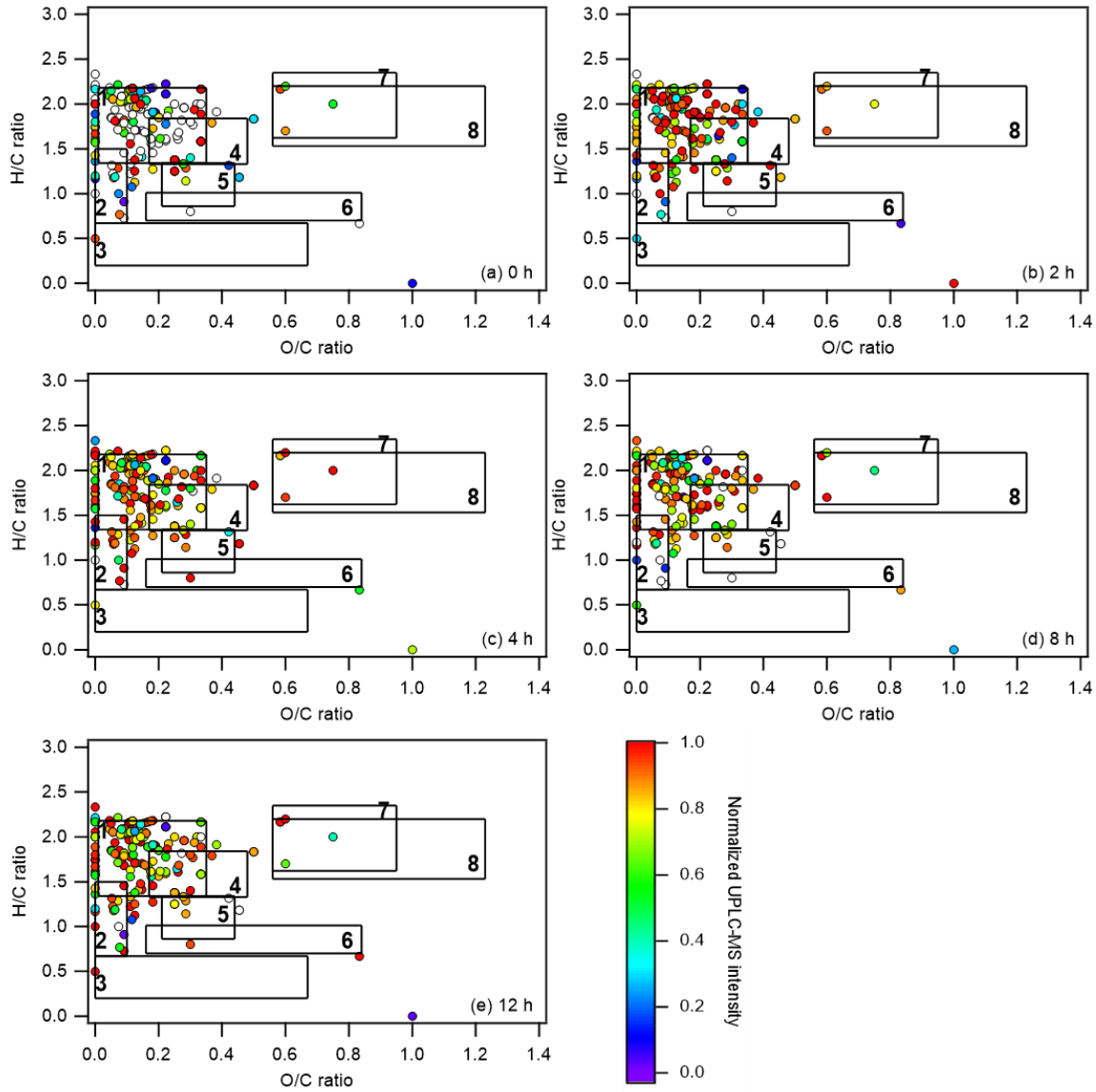

Figure S9. Van Krevelen diagrams of water-insoluble compounds from *E. hormaechei* B0910 during exposure to simulated sunlight at pH 4.3: (a) 0 h, (b) 2 h, (c) 4 h, (d) 8 h, and (e) 12 h. The color of each symbol denotes its UPLC-MS intensity at that specific time point normalized to its maximum UPLC-MS intensity obtained during the entire experiment. Symbols that are colored white indicates that these compounds were not detected at that specific time point. The Van Krevelen diagrams are divided into eight chemical classes based on their O/C and H/C ratios: (1) lipids, (2) unsaturated hydrocarbons, (3) condensed aromatic structures, (4) peptides, (5) lignin, (6) tannin, (7) amino sugars, and (8) carbohydrates.

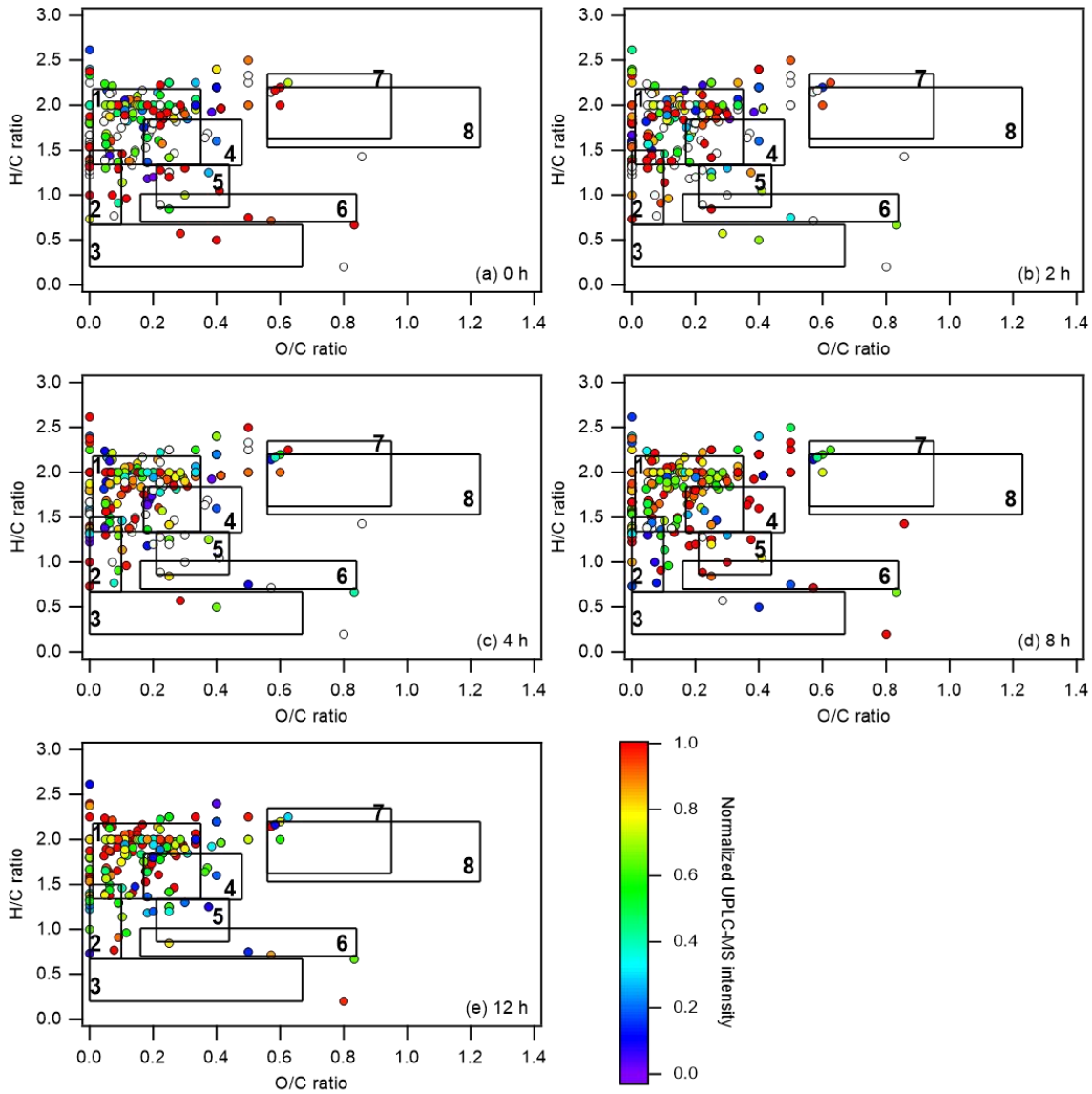

Figure S10. Van Krevelen diagrams of water-soluble compounds from *E. hormaechei* pf0910 during exposure to simulated sunlight at pH 4.3: (a) 0 h, (b) 2 h, (c) 4 h, (d) 8 h, and (e) 12 h. The color of each symbol denotes its UPLC-MS intensity at that specific time point normalized to its maximum UPLC-MS intensity obtained during the entire experiment. Symbols that are colored white indicates that these compounds were not detected at that specific time point. The Van Krevelen diagrams are divided into eight chemical classes based on their O/C and H/C ratios: (1) lipids, (2) unsaturated hydrocarbons, (3) condensed aromatic structures, (4) peptides, (5) lignin, (6) tannin, (7) amino sugars, and (8) carbohydrates.

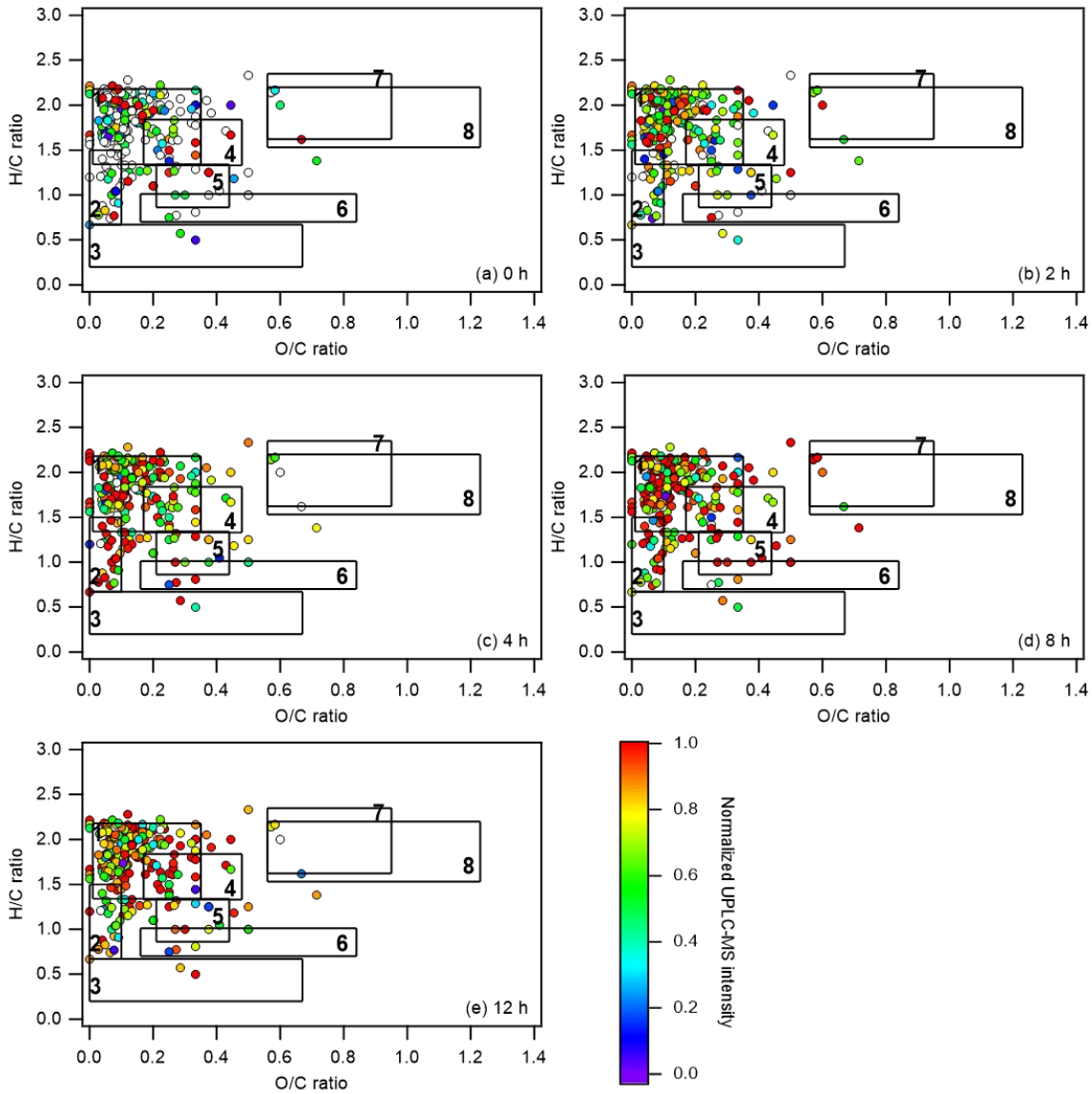

Figure S11. Van Krevelen diagrams of water-insoluble compounds from *E. hormaechei* pf0910 during exposure to simulated sunlight at pH 4.3: (a) 0 h, (b) 2 h, (c) 4 h, (d) 8 h, and (e) 12 h. The color of each symbol denotes its UPLC-MS intensity at that specific time point normalized to its maximum UPLC-MS intensity obtained during the entire experiment. Symbols that are colored white indicates that these compounds were not detected at that specific time point. The Van Krevelen diagrams are divided into eight chemical classes based on their O/C and H/C ratios: (1) lipids, (2) unsaturated hydrocarbons, (3) condensed aromatic structures, (4) peptides, (5) lignin, (6) tannin, (7) amino sugars, and (8) carbohydrates.

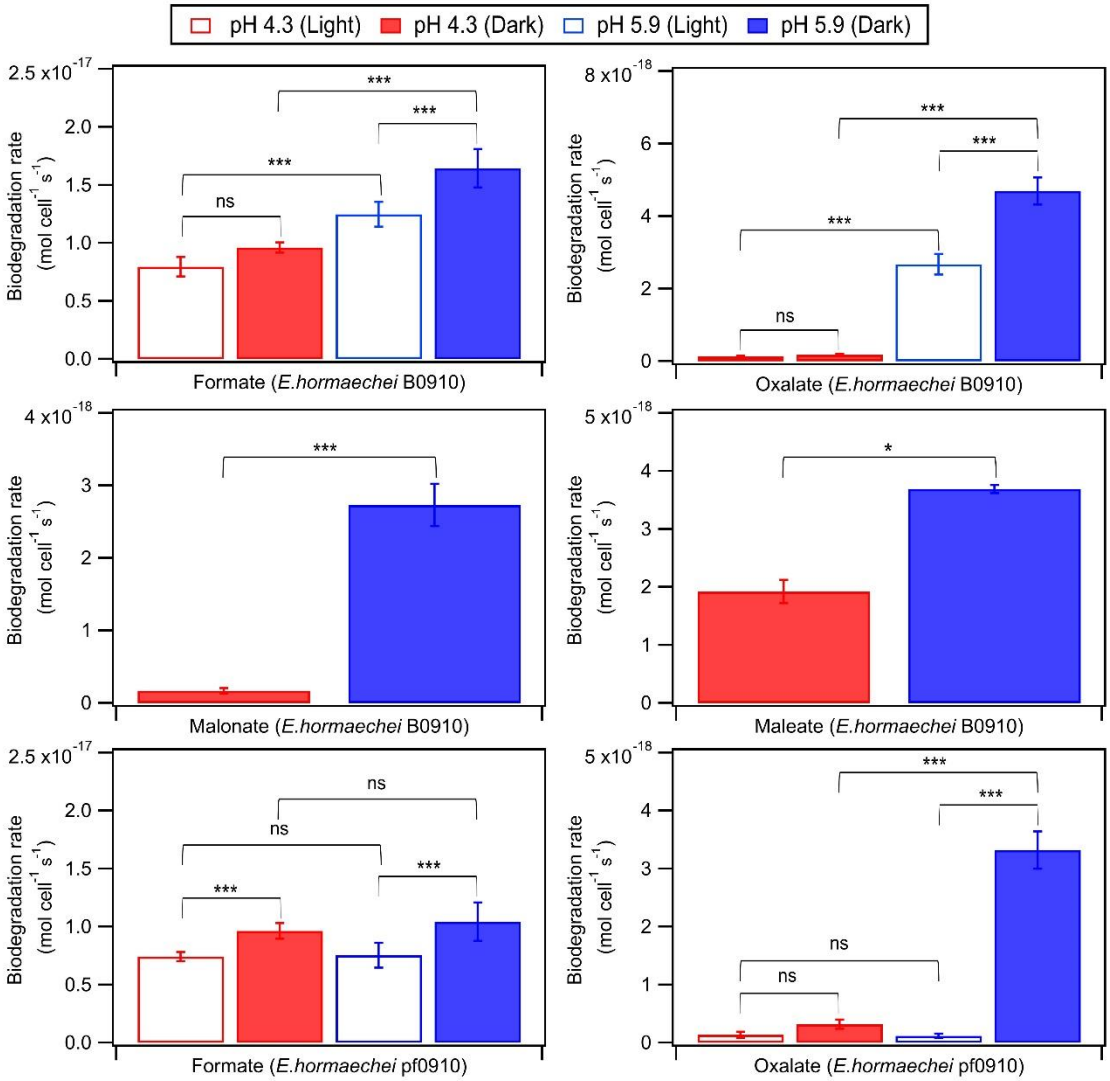

Figure S12. Biodegradation rates of oxalate, maleate, and malonate by (a) *E. hormaechei* B0910 and (b) *E. hormaechei* pf0910 under light and dark conditions at pH 4.3 and pH 5.9. Error bars represent one standard deviation from the mean of biological triplicates. Statistical analysis was performed using the Student's t test (ns: not significant, *: p value < 0.05, **: p value < 0.01, ***: p value < 0.001).

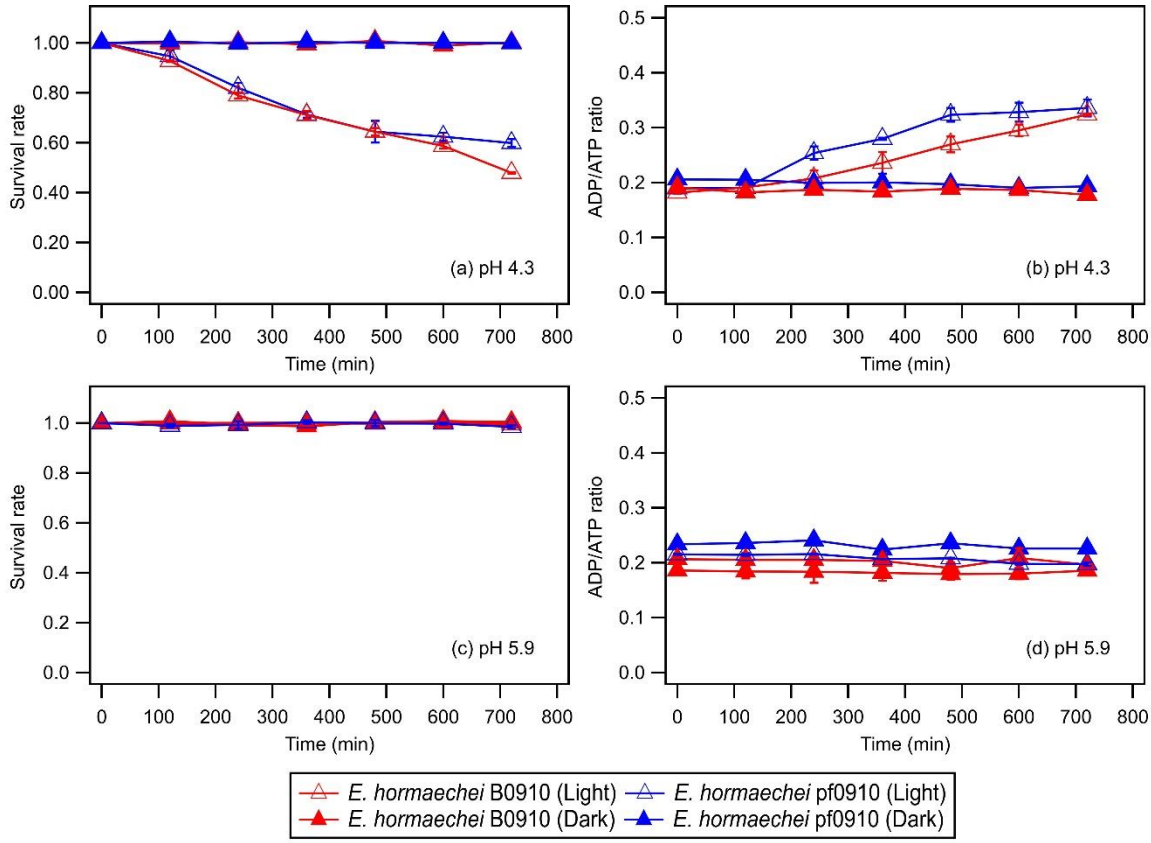

Figure S13. Survival and ADP/ATP ratios of *E. hormaechei* B0910 and *E. hormaechei* pf0910 under illuminated and dark conditions at pH 4.3 and pH 5.9 in the solutions containing the seven organic acids. Error bars represent one standard deviation from the mean of biological triplicates.

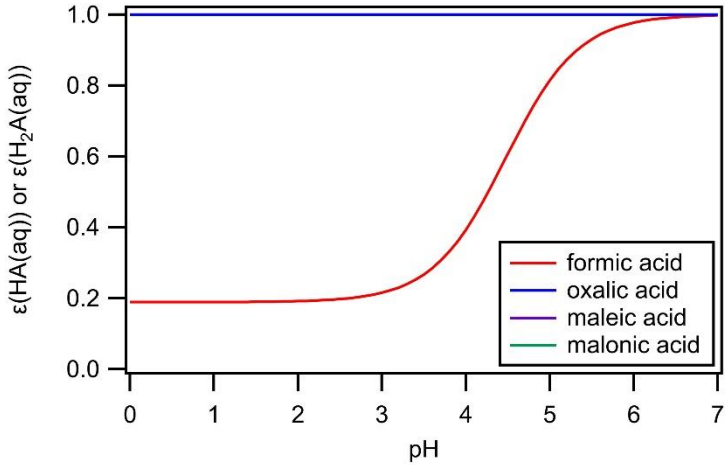

Figure S14. Calculated pH-dependent molar fraction of formic acid in the aqueous phase ($\varepsilon(HA(aq))$) and pH-dependent molar fractions of oxalic acid, malonic acid, and maleic acid in the aqueous phase ($\varepsilon(H_2A(aq))$) under cloud water conditions (Section S6 and Table S8). A liquid water concentration of 10^6 μg m^{-3} (Ervens et al., 2011) was assumed in these calculations. A significant fraction of formic acid will be in the gas phase at pH 4 and 5 under cloud water conditions, whereas all of the oxalic acid, malonic acid, and maleic acid will be in the aqueous phase at pH 4 and 5 under cloud water conditions (note that their values overlap one another at $\varepsilon(H_2A(aq)) = 1$). These differences were due primarily to the large differences in their water solubility (i.e., Henry's law constants) (Table S8).

Table S1. Chemical composition of the artificial cloud water used to prepare bacterial cells and perform experiments that investigated the effects of cloud water pH and light exposure on the survival and energetic metabolism of bacteria. In the experiments, the pH of the artificial cloud water was adjusted while keeping the final organic and inorganic ion composition the same.

Organic ion	μM	Inorganic ion	μM
Formate	17.1	Na^+	93
Acetate	10.2	NH_4^+	235
Pyruvate	2.7	K^+	8
Oxalate	10.3	Mg^{2+}	23
		Ca^{2+}	49
		Cl^-	138
		SO_4^{2-}	305

Table S2. Chemical composition of the artificial cloud water used for organic acid biodegradation experiments.

Organic ion	μM	Inorganic ion	μM
Formate	50	Na^+	930
Acetate	50	NH_4^+	2350
Pyruvate	50	K^+	80
Oxalate	50	Mg^{2+}	230
Succinate	50	Ca^{2+}	490
Maleate	50	Cl^-	1380
Malonate	50	SO_4^{2-}	3050
Glutarate	50		
MSA	50		

Table S3. Genes involved in the pH homeostasis in the two *E. hormaechei* strains.

Transporters	Protein subunits	*E. hormaechei B0910*	*E. hormaechei pf0910*
		CDS	CDS
F1F0-type ATP synthase	Subunit a, AtpB	MOG78_16595	MMW20_13045
	Subunit c, AtpE	MOG78_16590	MMW20_13050
	Subunit b, AtpF	MOG78_16585	MMW20_13055
	Subunit delta, AtpH	MOG78_16580	MMW20_13060
	Subunit alpha, AtpA	MOG78_16575	MMW20_13065
	Subunit gamma, AtpG	MOG78_16570	MMW20_13070
	Subunit beta, AtpD	MOG78_16565	MMW20_13075
	Subunit epsilon, AtpC	MOG78_16560	MMW20_13080
Kdp-type high-affinity potassium transporter	Potassium-binding ATPase subunit KdpA	MOG78_10080	MMW20_19865
	Potassium-binding ATPase subunit KdpB	MOG78_10085	MMW20_19860
	Potassium-binding ATPase subunit KdpC	MOG78_10090	MMW20_19855
	Potassium-binding ATPase subunit KdpF	MOG78_10075	Gene sequence found but CDS is not annotated. (Chromosome genome nucleotide position: 3800683-3800772)
Kup-type low-affinity potassium transporter	Kup	MOG78_16640	MMW20_13000

167 **Table S4.** Stoichiometric ranges of the eight chemical classes in VK diagrams (Bauer et al.,
168 2002; Jaenicke, 2005).

Chemical class	H/C	O/C
Amino sugar (Burrows et al., 2009)	$1.62 \leq H/C \leq 2.35$	$0.56 \leq O/C \leq 0.95$
Carbohydrate (Jaenicke, 2005)	$1.53 \leq H/C \leq 2.20$	$0.56 \leq O/C \leq 1.23$
Lignin (Möhler et al., 2007)	$0.86 \leq H/C \leq 1.34$	$0.21 \leq O/C \leq 0.44$
Lipid (Burrows et al., 2009)	$1.34 \leq H/C \leq 2.18$	$0.01 \leq O/C \leq 0.35$
Peptide (Attard et al., 2012)	$1.33 \leq H/C \leq 1.84$	$0.17 \leq O/C \leq 0.48$
Tannin (Hu et al., 2018)	$0.70 \leq H/C \leq 1.01$	$0.16 \leq O/C \leq 0.84$
Unsaturated hydrocarbons (Amato et al., 2005)	$0.67 \leq H/C \leq 1.5$	$0 \leq O/C \leq 0.10$
Condensed aromatic structures (Delort et al., 2010)	$0.20 \leq H/C \leq 0.67$	$0 \leq O/C \leq 0.67$

169

Table S5. Genes involved in the biodegradation of organic acids in the two *E. hormaechei* strains.

Organic acid	Genes	*E. hormaechei B0910*		*E. hormaechei pf0910*	
		Biodegradation	**CDS**	**Biodegradation**	**CDS**
		Yes/No	**Absent/Present**	**Yes/No**	**Absent/Present**
Formic acid	Formate dehydrogenase	Yes	MOG78_16880; MOG78_16875; MOG78_16870; MOG78_06810	Yes	MMW20_12765; MMW20_12770; MMW20_12775; MMW20_22665
Oxalic acid	Oxalate decarboxylase	Yes	Absent	Yes	Absent
	Oxalate oxidase	Yes	Absent	Yes	Absent
	Formyl-CoA:oxalate CoA-transferase	Yes	Absent	Yes	Absent
	Succinyl-CoA:oxalate CoA-transferase	Yes	Absent	Yes	Absent
	Hypothetical protein (Cupin 2 protein)[a]	Yes	MOG78_20825	Yes	MMW20_08875
Malonic acid	Malonate decarboxylase	Yes	MOG78_18565; MOG78_18550; MOG78_18545; MOG78_18540; MOG78_18530	No	MMW20_11060; MMW20_11075; MMW20_11080; MMW20_11085; MMW20_11095
	Malonate CoA-transferase	Yes	Absent	No	Absent
	Malonate-semialdehyde dehydrogenase	Yes	Absent	No	Absent
	Malonyl-CoA/methylmalonyl-CoA synthetase	Yes	Absent	No	Absent
Maleic acid	Maleate isomerase	Yes	Absent	No	Absent
	Maleate hydratase	Yes	Absent	No	Absent
	3-isopropylmalate dehydratase[a]	Yes	MOG78_13080; MOG78_13075	No	MMW20_17000; MMW20_17005
Acetic acid	Acetyl-CoA synthetase	No	MOG78_14765	No	MMW20_14980
	Acetate kinase	No	MOG78_01250	No	MMW20_05785
	Aldehyde dehydrogenase	No	MOG78_17415	No	MMW20_12230
	ActP[b]	No	MOG78_14775	No	MMW20_14970

	SatP[b]	No	MOG78_13285	No	MMW20_16750
Methane sulfonic acid	Alkanesulfonate monooxygenase	No	MOG78_08820; MOG78_08810	No	MMW20_21175; MMW20_21185
Glutaric acid	Succinate-semialdehyde dehydrogenase / glutarate-semialdehyde dehydrogenase[c]	No	MOG78_19060; MOG78_13695	No	MMW20_10560; MMW20_16345
	Glutaryl-CoA synthetase	No	Absent	No	Absent
	Glutarate dioxygenase	No	Absent	No	Absent

[a] Genes are not canonical but may involve in the biodegradation of organic acids.

[b] Transporter proteins involved in uptake of acetic acid for biodegradation

[c] No reverse catalysis in the direction from glutarate to glutarate-semialdehyde has been reported in the literature.

Table S6. Concentration of radicals and cells used to estimate the loss rates by biodegradation and chemical reactions in Table S6.

Radical concentration/ Cell concentration	Area	Concentration	Reference
·OH (M)	Remote	2.2×10^{-14}	(Vaitilingom et al., 2010)
	Marine	2.0×10^{-12}	(Vaitilingom et al., 2013)
	Urban	3.5×10^{-15}	(Morris et al., 2014)
NO_3· (M)	Remote	5.1×10^{-15}	(Morris et al., 2017)
	Marine	6.9×10^{-15}	(Hu et al., 2018)
	Urban	1.4×10^{-13}	(Huang et al., 2021)
Cell (cell L^{-1})		8.0×10^{7}	(Zhang et al., 2021)

Table S7. Estimations of the loss rates of formate, oxalate, and malonate by biodegradation and chemical reactions (i.e., ·OH oxidation (daytime) and NO_3· (nighttime)). These loss rates were calculated based on concentrations and pH measured at the different sites. Equations used in these calculations can be found in Section S6. References used to obtain the pH of cloud/rainwater and organic acids are indicated in superscripts. The biodegradation and chemical reaction loss rates calculated here were used to generate Figure 5.

Daytime

Location (remote)	Category	pH	Formate (μM)	Formate loss rate (M s^{-1})			Oxalate (μM)	Oxalate loss rate (M s^{-1})		
				bio (pH ~4)	bio (pH ~5)	·OH (remote)		bio (pH ~4)	bio (pH ~5)	·OH (remote)
Mount Lu(Möhler et al., 2007)	Cloud	3.81 (Vaïtilingom et al., 2012)	10.83 (Wei et al., 2017)	1.34×10^{-10}		5.72×10^{-10}	4.95 (Zhu et al., 2018)	1.06×10^{-12}		1.74×10^{-11}
Mount Lu(Wei et al., 2017)	Rain	4.44 (Peng et al., 2019)	10.21 (Amato et al., 2005)	1.26×10^{-10}		5.39×10^{-10}	2.54 (Burrows et al., 2009)	5.44×10^{-13}		8.92×10^{-12}
Mount Heng(Amato et al., 2017)	Cloud	3.8 (Amato et al., 2005)	19.65 (Amato et al., 2017)	2.43×10^{-10}		1.04×10^{-9}	5.11 (Wei et al., 2017)	1.10×10^{-12}		1.80×10^{-11}
Mount Heng(Delort et al., 2010)	Rain	4.35 (Vaitilingom et al., 2010)	14.30 (Vaitilingom et al., 2013)	1.77×10^{-10}		7.55×10^{-10}	1.66 (Ervens and Amato, 2020)	3.55×10^{-13}		5.83×10^{-12}
Mangdang Mountain(Ariya et al., 2002)	Rain	4.81 (Husárová et al., 2011)	7.90 (Vaïtilingom et al., 2011)	9.78×10^{-11}		4.17×10^{-10}	1.80 (Jaber et al., 2020)	3.86×10^{-13}		6.34×10^{-12}
Taiwan(Jaber et al., 2021)	Cloud	3.91 (Joly et al., 2015)	5.74 (Davey and O'toole, 2000)	7.11×10^{-11}		3.03×10^{-10}	6.60 (Delort et al., 2010)	1.42×10^{-12}		2.32×10^{-11}
Kleiner Feldberg, Germany(Flemming and Wingender, 2010)	Cloud	3.9-4.6 (Vaïtilingom et al., 2012)	3.26 (Matulova et al., 2014)	4.03×10^{-11}		1.72×10^{-10}	ND			
Whiteface Mountain, USA(Amato et al., 2005)	Cloud	3.1-4.4 (Peng et al., 2019)	25.20 (Amato et al., 2005)	3.12×10^{-10}		1.33×10^{-9}	9.66 (Pye et al., 2020)	2.07×10^{-12}		3.40×10^{-11}
Rax, Austria(Shah et al., 2020)	Cloud	3.84 (Li et al., 2020)	13.25 (Pye et al., 2020)	1.64×10^{-10}		7.00×10^{-10}	5.11 (Shah et al., 2020)	1.10×10^{-12}		1.80×10^{-11}
Sonnblick, Austria(Qu and Han, 2021)	Cloud	5.0-6.5 (Anglada et al., 2015)	6.30 (Joly et al., 2015)		9.79×10^{-11}	3.33×10^{-10}	1.89 (Vaïtilingom et al., 2011)		3.61×10^{-12}	6.65×10^{-12}
Mount Tai, China(Joly et al., 2015)	Cloud	4.6 (Jaber et al., 2021)	31.80 (Jaber et al., 2020)	3.94×10^{-10}		1.68×10^{-9}	11.10 (Li et al., 2020)	2.38×10^{-12}		3.91×10^{-11}
Shangzhong(Qu and Han, 2021)	Rain	ND	4.95 (Peng et al., 2019)	6.13×10^{-11}		2.61×10^{-10}	1.16 (Chen et al., 2012)	2.48×10^{-13}		4.07×10^{-12}
São Paulo State, Brazil(Després et al., 2012)	Rain	4.96 (Ding et al., 2015)	7.80 (Zhou et al., 2018)		1.21×10^{-10}	4.12×10^{-10}	1.20 (Prokof'eva et al., 2021)		2.29×10^{-12}	4.22×10^{-12}

Location (Marine)	Category	pH	Formate (μM)	Formate loss rate (M s^{-1})			Oxalate (μM)	Oxalate loss rate (M s^{-1})		
				bio (pH ~4)	bio (pH ~5)	·OH (marine)		bio (pH ~4)	bio (pH ~5)	·OH (marine)
Puerto Rico	Cloud	5.5 (Romano et al., 2019)	1.00 (Ruiz-Gil et al., 2020)		1.55×10^{-11}	4.80×10^{-9}	0.50 (Romano et al., 2021)		9.55×10^{-13}	1.60×10^{-10}
Puerto Rico(Tsai and Kuo, 2013)	Rain	5.3 (Löflund et al., 2002)	0.20 (Sun et al., 2016)		3.11×10^{-12}	9.60×10^{-10}	0.00 (Li et al., 2020)			

Puy de dome(Vaitilingom et al., 2010)	Cloud	6.1 (Vaïtilingom et al., 2011)	4.90 (George et al., 2015)		7.61×10^{-11}	2.35×10^{-8}	1.00 (Huang et al., 2018)			1.91×10^{-12}	3.20×10^{-10}

Location (Urban)			Formate (μM)	Formate loss rate (M s^{-1})			Oxalate (μM)	Oxalate loss rate (M s^{-1})			
				bio (pH ~4)	bio (pH ~5)	·OH (urban)		bio (pH ~4)	bio (pH ~5)	·OH (urban)	
Shenzhen, South China(Misovich et al., 2021)	Rain	4.56 (Li et al., 2020)	2.26 (Tsai and Kuo, 2013)	2.80×10^{-11}		1.90×10^{-11}	0.58 (Löflund et al., 2002)	1.23×10^{-13}		3.22×10^{-13}	
Anshun(Sun et al., 2016)	Rain	4.67 (Li et al., 2020)	8.77 (Vaitilingom et al., 2010)	1.09×10^{-10}		7.37×10^{-11}	2.84 (Jaber et al., 2020)	6.09×10^{-13}		1.59×10^{-12}	
Newark US East Coast(Jaber et al., 2021)	Rain	4.6 (Vaïtilingom et al., 2011)	4.44 (Jaber et al., 2020)	5.50×10^{-11}		3.73×10^{-11}	0.68 (Jaber et al., 2021)	1.46×10^{-13}		3.81×10^{-13}	
Hong Kong SAR(Bearson et al., 1997)	Cloud	3.87 (Lund et al., 2014)	17.10 (Bearson et al., 1997)	2.12×10^{-10}		1.44×10^{-10}	10.30 (Davey and O'toole, 2000)	2.21×10^{-12}		5.77×10^{-12}	
Puy de dome(Delort et al., 2010)	Cloud	3.9 (Flemming and Wingender, 2010)	33.20 (Vaïtilingom et al., 2012)	4.11×10^{-10}		2.79×10^{-10}	9.30 (Matulova et al., 2014)	1.99×10^{-12}		5.21×10^{-12}	

ND: No data

Nighttime

Location (remote)	Category	pH	Formate (μM)	Formate loss rate (M s^{-1})			Oxalate (μM)	Oxalate loss rate (M s^{-1})			Malonate (μM)	Malonate loss rate (M s^{-1})		
				bio (pH ~4)	bio (pH ~5)	$NO_3\cdot$ (remote)		bio (pH ~4)	bio (pH ~5)	$NO_3\cdot$ (remote)		bio (pH ~4)	bio (pH ~5)	$NO_3\cdot$ (remote)
Mount Lu(Guan and Liu, 2020)	Cloud	3.81 (Davey and O'toole, 2000)	10.83 (Delort et al., 2010)	1.69×10^{-10}		2.32×10^{-12}	4.95 (Flemming and Wingender, 2010)	2.07×10^{-12}		1.11×10^{-12}	ND			
Mount Lu(Vaïtilingom et al., 2012)	Rain	4.44 (Matulova et al., 2014)	10.21 (Bianco et al., 2018)	1.59×10^{-10}		2.19×10^{-12}	2.54 (Laszakovits and Mackay, 2022)	1.06×10^{-12}		5.69×10^{-13}	ND			
Mount Heng(Watson et al., 2007)	Cloud	3.8 (Rivas-Ubach et al., 2018)	19.65 (Matulova et al., 2014)	3.06×10^{-10}		4.21×10^{-12}	5.11 (Bianco et al., 2016)	2.14×10^{-12}		1.15×10^{-12}	ND			
Mount Heng(Tyagi et al., 2015)	Rain	4.35 (Jaber et al., 2021)	14.30 (Bianco et al., 2019)	2.23×10^{-10}		3.06×10^{-12}	1.66 (Vaitilingom et al., 2010)	6.94×10^{-13}		3.71×10^{-13}	ND			
Mangdang Mountain(Vaïtilingom et al., 2011)	Rain	4.81 (Fankhauser et al., 2019)	7.90 (Makuc et al., 2001)	1.23×10^{-10}		1.69×10^{-12}	1.80 (Tilgner et al., 2021)	7.55×10^{-13}		4.04×10^{-13}	1.40 (Koutny et al., 2006)		5.16×10^{-12}	4.00×10^{-14}
Taiwan(Guan and Liu, 2020)	Cloud	3.91 (Vaïtilingom et al., 2011)	5.74 (Jaber et al., 2020)	8.95×10^{-11}		1.23×10^{-12}	6.60 (Jaber et al., 2021)	2.77×10^{-12}		1.48×10^{-12}	0.16 (Herrmann et al., 2010)	3.65×10^{-14}		4.57×10^{-15}

Kleiner Feldberg, Germany(Vaïtilingom et al., 2011)	Cloud	3.9-4.6 (Jaber et al., 2020)	3.26 (Jaber et al., 2021)	5.08×10^{-11}		6.98×10^{-13}	ND				ND			
Whiteface Mountain, USA(Herrmann et al., 2010)	Cloud	3.1-4.4 (Ervens et al., 2003)	25.20 (Herrmann et al., 2010)	3.93×10^{-10}		5.40×10^{-12}	9.66 (Vaitilingom et al., 2010)	4.05×10^{-12}		2.17×10^{-12}	7.69 (Vaïtilingom et al., 2011)	1.75×10^{-12}		2.20×10^{-13}
Rax, Austria(Fankhauser et al., 2019)	Cloud	3.84 (Pye et al., 2020)	13.25 (Li et al., 2020)	2.07×10^{-10}		2.84×10^{-12}	5.11 (Pye et al., 2020)	2.14×10^{-12}		1.15×10^{-12}	1.92 (Shah et al., 2020)	4.38×10^{-13}		5.49×10^{-14}
Sonnblick, Austria(Qu and Han, 2021)	Cloud	5.0-6.5 (Vaïtilingom et al., 2012)	6.30 (Zhu et al., 2018)		1.32×10^{-10}	1.35×10^{-12}	1.89 (Peng et al., 2019)		1.19×10^{-11}	4.24×10^{-13}	0.38 (Ariya et al., 2002)		1.42×10^{-12}	1.10×10^{-14}
Mount Tai, China(Vaitilingom et al., 2010)	Cloud	4.6 (Husárová et al., 2011)	31.80	4.96×10^{-10}		6.81×10^{-12}	11.10 (Vaïtilingom et al., 2011)	4.65×10^{-12}		2.49×10^{-12}	ND			
Shangzhong(Xu et al., 2009)	Rain		4.95	7.71×10^{-11}		1.06×10^{-12}	1.16	4.84×10^{-13}		2.59×10^{-13}	ND			
São Paulo State, Brazil(Coelho et al., 2011)	Rain	4.96 (Coelho et al., 2011)	7.80 (Coelho et al., 2011)		1.63×10^{-10}	1.67×10^{-12}	1.20 (Coelho et al., 2011)		7.57×10^{-12}	2.69×10^{-13}	ND			

				Formate loss rate ($M\ s^{-1}$)				Oxalate loss rate ($M\ s^{-1}$)				Malonate loss rate ($M\ s^{-1}$)		
Location (marine)		pH	Formate (μM)	bio (pH ~4)	bio (pH ~5)	$NO_3\cdot$ (marine)	Oxalate (μM)	bio (pH ~4)	bio (pH ~5)	$NO_3\cdot$ (marine)	Malonate (μM)	bio (pH ~4)	bio (pH ~5)	$NO_3\cdot$ (marine)
Puerto Rico(Gioda et al., 2011)	Cloud	5.5 (Gioda et al., 2011)	1.00 (Gioda et al., 2011)		2.09×10^{-11}	2.90×10^{-13}	0.50 (Gioda et al., 2011)		3.16×10^{-12}	1.52×10^{-13}	ND			
	Rain	5.3 (Gioda et al., 2011)	0.20 (Gioda et al., 2011)		4.19×10^{-12}	5.80×10^{-14}	ND				ND			
Puy de dôme(Vaitilingom et al., 2013)	Cloud	6.1 (Vaitilingom et al., 2013)	4.90 (Vaitilingom et al., 2013)		1.03×10^{-10}	1.42×10^{-12}	1.00 (Vaitilingom et al., 2013)		6.31×10^{-12}	3.04×10^{-13}	0.40 (Vaïtilingom et al., 2012)		1.47×10^{-12}	1.55×10^{-14}

				Formate loss rate ($M\ s^{-1}$)				Oxalate loss rate ($M\ s^{-1}$)				Malonate loss rate ($M\ s^{-1}$)		
Location (urban)		pH	Formate (μM)	bio (pH ~4)	bio (pH ~5)	$NO_3\cdot$ (urban)	Oxalate (μM)	bio (pH ~4)	bio (pH ~5)	$NO_3\cdot$ (urban)	Malonate (μM)	bio (pH ~4)	bio (pH ~5)	$NO_3\cdot$ (urban)
Shenzhen, South China(Huang et al., 2010)	Rain	4.56 (Huang et al., 2010)	2.26 (Huang et al., 2010)	3.52×10^{-11}		1.33×10^{-11}	0.58 (Huang et al., 2010)	2.41×10^{-13}		3.54×10^{-12}	ND			
Anshun(Zhang et al., 2011)	Rain	4.67 (Zhang et al., 2011)	8.77 (Zhang et al., 2011)	1.37×10^{-10}		5.16×10^{-11}	2.84 (Zhang et al., 2011)	1.19×10^{-12}		1.75×10^{-11}	ND			
Newark US East Coast(Song and Gao, 2009)	Rain	4.6 (Song and Gao, 2009)	4.44 (Song and Gao, 2009)	6.92×10^{-11}		2.61×10^{-11}	0.68 (Song and Gao, 2009)	2.85×10^{-13}		4.19×10^{-12}	0.29(Song and Gao, 2009)	6.61×10^{-14}		2.27×10^{-13}
Hong Kong SAR(Li et al., 2020)	Cloud	3.87 (Li et al., 2020)	17.10 (Li et al., 2020)	2.66×10^{-10}		1.01×10^{-10}	10.30 (Li et al., 2020)	4.32×10^{-12}		6.34×10^{-11}	1.36 (Zhao et al., 2019)	3.10×10^{-13}		1.07×10^{-12}
Puy de dome(Vaitilingom et al., 2013)	Cloud	3.9 (Vaitilingom et al., 2013)	33.20 (Vaitilingom et al., 2013)	5.17×10^{-10}		1.95×10^{-10}	9.30 (Vaitilingom et al., 2013)	3.90×10^{-12}		5.73×10^{-11}	3.50 (Vaitilingom et al., 2013)	7.97×10^{-13}		2.74×10^{-12}

187 ND: No data

Table S8. Acid dissociation constants and Henry's law coefficients at 25 °C used to generate $\varepsilon(HA(aq))$ and $\varepsilon(H_2A(aq))$ S curves in Figure S14

Organic acid	First acid dissociation constant (K_{a1}) (mol L^{-1})	Second acid dissociation constant (K_{a2}) (mol L^{-1})	Henry's law constant (H_{HA} or H_{H_2A}) (mol L^{-1} atm^{-1})
Formic acid	1.78×10^{-4} (Haynes, 2014)	Not applicable	9.53×10^{3}
Oxalic acid	5.62×10^{-2} (Haynes, 2014)	1.55×10^{-4} (Haynes, 2014)	6.11×10^{8} (Nah et al., 2018)[a]
Malonic acid	1.48×10^{-3} (Williams, 2022)	2.04×10^{-6} (Williams, 2022)	3.85×10^{10} (Compernolle and Müller, 2014)
Maleic acid	1.26×10^{-2} (Weast and Astle, 1981)	8.51×10^{-7} (Weast and Astle, 1981)	1.42×10^{10} (Lide and Frederikse, 1995)

[a]While we used the Henry's law coefficient provided by Nah et al. (2018), it should be noted that the authors obtained this value by taking the average of $H_{C_2H_2O_4}$ values provided by Clegg et al. (1996), Compernolle and Muller (2014) and Saxena and Hildemann (1996), and accounted for the effect of temperature using the equations provided by Sander (2015).

Section S1. Genome assembly, annotation, and taxonomic analysis

Genome assembly of the sequencing reads was performed using the NECAT pipeline (v0.0.1_update20200803) (Chen et al., 2021) with the default parameters. The reads were first corrected (PREP_OUTPUT_COVERAGE = 40, CNS_OUTPUT_COVERAGE = 30, MIN_READ_LENGTH = 3000) and then the corrected reads were assembled (OVLP_FAST_OPTIONS = -n 500 -z 20 -b 2000 -e 0.5 -j 0 -u 1 -a 1000, OVLP_SENSITIVE_OPTIONS = -n 500 -z 10 -e 0.5 -j 0 -u 1 -a 1000). Both the correction and assembly steps were progressive with multiple processing steps to improve the accuracy and completeness. The quality of the assembled genomes was evaluated using the Benchmarking Universal Single-copy Orthologs (BUSCO v5.3.1) tool based on the database of enterobacterales_odb10 (Manni et al., 2021). For both strains B00910 and pf0910, complete circular chromosomes and plasmids were obtained.

Genome annotation was performed using Prokka (v1.14.6) (Seemann, 2014) with the default parameters. Whole genome-based taxonomic analysis was conducted using the Type

(Strain) Genome Server (TYGS) (Meier-Kolthoff and Göker, 2019). Average Nucleotide Identity (ANI) was calculated by fastANI (v1.33) (Jain et al., 2018). Metabolic pathways were analyzed using the KEGG Mapper (Kanehisa et al., 2022) and the RAST server (Aziz et al., 2008). The sequences of the two genomes have been deposited in NCBI under the BioProject number PRJNA812965.

Section S2. Extraction of water-insoluble and water-soluble biological material and organic compounds for UPLC-MS analysis

A modified Bligh & Dyer (BD) protocol was performed to extract water-insoluble organic compounds (Sündermann et al., 2016). Briefly, 3 mL of methanol (Duskan, LC-MS grade)/chloroform (RCI, HPLC grade) (1:2, v/v) was added to a filtered 5 mL sample solution and vortexed for 5 min, after which the samples were centrifuged at 3000 rpm for 10 min at 10 ℃. The bottom layer was collected into a clean 2 mL centrifuge tube and dried in a concentrator using nitrogen gas. The dried extracts were redissolved in 500 µL of acetonitrile (Duskan, LC-MS grade) and stored at -20 ℃ prior to UPLC-MS analysis. Solid-phase extraction (SPE) was performed to remove the inorganic salts and extract the water-soluble organic compounds using hydrophobic lipophilic balanced (HLB) cartridges (Oasis HLB, 6cc 500 mg). The HLB cartridges were first preconditioned with 1 mL methanol and 2 mL Milli-Q water. A 10 mL filtered sample solution was then loaded into the SPE cartridge and washed with 20 mL Milli-Q water under vacuum at a flow rate of 5 mL/min. The elution was performed by adding 1.5 mL methanol (Duskan, LC-MS grade). The eluent was evaporated to dryness under nitrogen gas and reconstituted in 500 µL acetonitrile (Duskan, LC-MS grade).

Section S3. UPLC-MS operation, data processing, and statistical analysis

Chromatographic separation was performed on a Kinetex HILIC LC column (100 × 2.1 mm, 2.6 µm, 100 Å, Phenomenex). The flow rate was fixed at 0.3 mL/min with ultra-pure water containing 5 mM ammonium acetate (Fisher, LC-MS grade) as mobile phase A and acetonitrile (Duskan, LC-MS grade) for mobile phase B. The following gradient program was used: 0 to 2 min 95% A; 2 to 4 min linear gradient to 80% B; 4 to 11 min linear gradient to

65% B; 11 to 12.5 min 65% B; 12.5 to 13 min linear gradient to 95% B; 13 to 15 min equilibration wash with 95% B. Injection volume was set at 10 uL. The information dependent analysis (IDA) acquisition was acquired with MS scan (100 to 1200 m/z) followed by MS/MS scan (50 to 1200 m/z) in positive ion mode. The following MS conditions were used: 30 PSI curtain gas, 60 PSI ion source gas, 3000 V ESI ion spray voltage, 320 ℃ source temperature, 10 V collision energy for MS, and 80 V declustering potential. MS/MS was acquired with a collision energy was 20 V with 5 V spread. The raw MS data was processed for peak detection, retention time correction, alignment, and integration using the XCMS software built into the web-based Galaxy platform (https://umsa.cerit-sc.cz/) (Gowda et al., 2014). The processed data was then uploaded to MetaboAnalyst 5.0 (https://www.metaboanalyst.ca/) (Pang et al., 2021) to identify cellular compounds that had prominent ion intensities.

The raw UPLC-MS data first underwent preprocessing, normalization, and quality control steps using the XCMS software built into the web-based Galaxy platform (available at: https://umsa.cerit-sc.cz/). The raw data was processed for peak detection, alignment, and framing. This generated a table that displayed the retention time, mass-to-charge ratio (m/z), and the intensity/peak area for each peak. The quality control step was performed to assess the stability of the intensities of peaks ("features") between samples. This was performed using quality control samples, which were mixtures of equal amounts of experimental samples taken at each time point of the experiment. The relative standard deviation (RSD) of each feature in the quality control sample was compared to those in the experimental samples. Features with higher RSD in the quality control sample than in the experimental samples were excluded, while features with RSD < 30% were retained for further analysis. Multivariable statistical analysis was performed on the retained features using principal component analysis (PCA) with 95% confidence ellipse and partial least squares discrimination analysis (PLS-DA) to identify potential discriminations between the experimental samples. Heatmaps were generated to determine how the retained features changed at different time points during the experiment. A selection of discriminant ions and buckets was done based on the variable importance in projection (VIP) values. Features with VIP values greater than 1.0 were used for the identification step. MS/MS analysis was performed for the structural identification of

compounds. The structure of each compound was deduced based on its adducts, isotopes, and MS/MS fragments using the SCIEX OS-Q software (AB Sciex). Information about compounds' chemical structures, m/z, and retention times were subsequently uploaded to MetaboAnalyst 5.0 (https://www.metaboanalyst.ca/), which used this information to identify the compounds.

Section S4. IC operation

Organic acid concentrations were measured using a Dionex ICS-1100 (ThermoFisher Scientific) system. Separation was achieved using a Dionex IonPac AS18 (4 × 250 mm) anion exchange column (Thermo Scientific) equipped with a Dionex IonPac AG18 (4 × 50 mm) guard column (Thermo Scientific). 16 mM potassium hydroxide (Fisher, ≥85%) was used as the mobile phase at a flow rate of 1.0 mL/min for a 30 min run time. Each aliquot of solution was passed through a syringe filter before IC analysis.

Section S5. Estimation of biodegradation and chemical reaction rates (M s^{-1}) in cloud water

S5.1. Biodegradation

The decay in the concentration of a specific organic acid as a function of time (0 to 12 hours) during a biodegradation experiment can be described by the following equation:

$$\frac{d[Acid]}{dt} = k'_{cell} \times [Acid] = k_{cell,acid} \times [cell]_{experiment} \times [Acid]_{experiment}$$

where k'_{cell} (s^{-1}) is the pseudo first order rate constant obtained from fitting the decay of the organic acid, and $[Acid]_{experiment}$ ($mol\ L^{-1}$) is the initial concentration of the organic acid used in the biodegradation experiment. k'_{cell} is the product of the concentration of bacteria cells used in the experiment ($[cell]_{experiment}, cell\ L^{-1}$) and the biodegradation rate constant ($k_{cell,acid}, L\ cell^{-1}s^{-1}$).

The loss rate of the organic acid in cloud water resulting from biodegradation is:

$$\frac{d[Acid]_{cloud}}{dt} = k_{cell,acid} \times [cell]_{cloud} \times [Acid]_{cloud}$$

where $[cell]_{cloud}$ $(cell\ L^{-1})$ is the concentration of bacteria cells present in cloud water, and $[Acid]_{cloud}$ $(mol\ L^{-1})$ is the concentration of the organic in cloud water.

S5.2. Chemical reactions

The loss rates of the organic acid in cloud water resulting from reactions with ·OH and NO_3· are:

$$\frac{d[Acid]_{cloud}}{dt} = k_{OH,acid} \times [\cdot OH]_{cloud} \times [Acid]_{cloud}$$

$$\frac{d[Acid]_{cloud}}{dt} = k_{NO3,acid} \times [NO_3 \cdot]_{cloud} \times [Acid]_{cloud}$$

where $k_{OH,acid}$ $(L\ mol^{-1}s^{-1})$ and $k_{NO3,acid}$ $(L\ mol^{-1}s^{-1})$ are the rate constants for the reactions of the organic acid with ·OH and NO_3·, respectively, and $[\cdot OH]_{cloud}$ $(mol\ L^{-1})$ and $[NO_3 \cdot]_{cloud}$ $(mol\ L^{-1})$ are the concentrations of ·OH and NO_3· in cloud water, respectively.

Section S6. Gas-aqueous phase partitioning of monocarboxylic and dicarboxylic acids

Meskhidze et al. (2003) and Guo et al. (2016) previously introduced the concept of "S curves", which describe how the pH of the aqueous phase affects the gas-aqueous partitioning of acidic and basic species. It is assumed that the equilibrium between gas and aqueous phases involves the dissolution of the acidic/basic species into the aqueous phase, followed by the dissociation of the dissolved species. Assuming unity activity coefficients, for monocarboxylic acids (HA, e.g., formic acid), the pH-dependence of the molar fraction of HA in the aqueous phase ($\varepsilon(HA(aq))$) is described by the following equation (Nah et al., 2018):

$$\varepsilon(HA(aq)) = \frac{H_{HA}WRT(10^{-pH} + K_{a1}) \times 0.987 \times 10^{-14}}{10^{-pH} + H_{HA}WRT(10^{-pH} + K_{a1}) \times 0.987 \times 10^{-14}}$$

where W is liquid water concentration (μg m^{-3}), H_{HA} (mole L^{-1} atm^{-1}) is the Henry's law constants for monocarboxylic acid, K_{a1} (mole L^{-1}) is the first acid dissociation constant, R is the gas constant (8.314 m^3 Pa K^{-1} mol^{-1}), and T is temperature (K). The complete derivation for $\varepsilon(HA(aq))$ can be found in the SI of Guo et al. (2015).

Assuming unity activity coefficients, for dicarboxylic acids (H_2A, e.g., oxalic acid,

malonic acid, and maleic acid), the pH-dependence of the molar fraction of H_2A in the aqueous phase ($\varepsilon(H_2A(aq))$) can eventually be simplified to the following equation (Nah et al., 2018):

$$\varepsilon(H_2A(aq)) \cong \frac{H_{H_2A}WRT(10^{-pH} + K_{a1}) \times 0.987 \times 10^{-14}}{10^{-pH} + H_{H_2A}WRT(10^{-pH} + K_{a1}) \times 0.987 \times 10^{-14}}$$

where W is liquid water concentration (μg m^{-3}), H_{H_2A} (mole L^{-1} atm^{-1}) is the Henry's law constants for monocarboxylic acid, K_{a1} (mole L^{-1}) is the first acid dissociation constant, R is the gas constant (8.314 m^3 Pa K^{-1} mol^{-1}), and T is temperature (K). The complete derivation for $\varepsilon(H_2A(aq))$ can be found in the SI of Nah et al. (2018), which also includes discussions of the assumptions made during the derivation process which will lead to the disappearance of the second acid dissociation constant (K_{a2}) term during the process of simplifying the equation.

References

Amato, P., Ménager, M., Sancelme, M., Laj, P., Mailhot, G., and Delort, A.-M.: Microbial population in cloud water at the Puy de Dôme: Implications for the chemistry of clouds, Atmospheric Environment, 39, 4143-4153, https://doi.org/10.1016/j.atmosenv.2005.04.002, 2005.

Amato, P., Joly, M., Besaury, L., Oudart, A., Taib, N., Mone, A. I., Deguillaume, L., Delort, A. M., and Debroas, D.: Active microorganisms thrive among extremely diverse communities in cloud water, PLoS One, 12, e0182869, 10.1371/journal.pone.0182869, 2017.

Anglada, J. M., Martins-Costa, M., Francisco, J. S., and Ruiz-Lopez, M. F.: Interconnection of reactive oxygen species chemistry across the interfaces of atmospheric, environmental, and biological processes, Accounts of chemical research, 48, 575-583, https://doi.org/10.1021/ar500412p, 2015.

Ariya, P. A., Nepotchatykh, O., Ignatova, O., and Amyot, M.: Microbiological degradation of atmospheric organic compounds, Geophysical Research Letters, 29, 34-31-34-34, 10.1029/2002gl015637, 2002.

Attard, E., Yang, H., Delort, A. M., Amato, P., Pöschl, U., Glaux, C., Koop, T., and Morris, C. E.: Effects of atmospheric conditions on ice nucleation activity of Pseudomonas, Atmospheric Chemistry and Physics, 12, 10667-10677, https://doi.org/10.5194/acp-12-10667-2012, 2012.

Aziz, R. K., Bartels, D., Best, A. A., DeJongh, M., Disz, T., Edwards, R. A., Formsma, K., Gerdes, S., Glass, E. M., and Kubal, M.: The RAST Server: rapid annotations using subsystems

technology, BMC genomics, 9, 1-15, https://doi.org/10.1186/1471-2164-9-75, 2008.

Bauer, H., Kasper-Giebl, A., Loflund, M., Giebl, H., Hitzenberger, R., Zibuschka, F., and Puxbaum, H.: The contribution of bacteria and fungal spores to the organic carbon content of cloud water, precipitation and aerosols, Atmospheric Research, 64, 109-119, https://doi.org/10.1016/s0169-8095(02)00084-4, 2002.

Bearson, S., Bearson, B., and Foster, J. W.: Acid stress responses in enterobacteria, Fems Microbiology Letters, 147, 173-180, https://doi.org/10.1111/j.1574-6968.1997.tb10238.x, 1997.

Bianco, A., Voyard, G., Deguillaume, L., Mailhot, G., and Brigante, M.: Improving the characterization of dissolved organic carbon in cloud water: Amino acids and their impact on the oxidant capacity, Sci Rep, 6, 37420, 10.1038/srep37420, 2016.

Bianco, A., Deguillaume, L., Chaumerliac, N., Vaitilingom, M., Wang, M., Delort, A. M., and Bridoux, M. C.: Effect of endogenous microbiota on the molecular composition of cloud water: a study by Fourier-transform ion cyclotron resonance mass spectrometry (FT-ICR MS), Sci Rep, 9, 7663, 10.1038/s41598-019-44149-8, 2019.

Bianco, A., Deguillaume, L., Vaitilingom, M., Nicol, E., Baray, J. L., Chaumerliac, N., and Bridoux, M.: Molecular Characterization of Cloud Water Samples Collected at the Puy de Dome (France) by Fourier Transform Ion Cyclotron Resonance Mass Spectrometry, Environmental Science & Technology, 52, 10275-10285, https://doi.org/10.1021/acs.est.8b01964, 2018.

Burrows, S. M., Elbert, W., Lawrence, M. G., and Poschl, U.: Bacteria in the global atmosphere - Part 1: Review and synthesis of literature data for different ecosystems, Atmospheric Chemistry and Physics, 9, 9263-9280, https://doi.org/10.5194/acp-9-9263-2009, 2009.

Chen, X., Ran, P., Ho, K., Lu, W., Li, B., Gu, Z., Song, C., and Wang, J.: Concentrations and Size Distributions of Airborne Microorganisms in Guangzhou during Summer, Aerosol and Air Quality Research, 12, 1336-1344, https://doi.org/10.4209/aaqr.2012.03.0066, 2012.

Chen, Y., Nie, F., Xie, S.-Q., Zheng, Y.-F., Dai, Q., Bray, T., Wang, Y.-X., Xing, J.-F., Huang, Z.-J., and Wang, D.-P.: Efficient assembly of nanopore reads via highly accurate and intact error correction, Nature Communications, 12, 1-10, https://doi.org/10.1038/s41467-020-20236-7, 2021.

Clegg, S. L., Brimblecombe, P., and Khan, L.: The Henry's law constant of oxalic acid and its partitioning into the atmospheric aerosol, Idojaras, 100, 51-68, 1996.

Coelho, C. H., Allen, A. G., Fornaro, A., Orlando, E. A., Grigoletto, T. L., and Campos, M. L. A.: Wet deposition of major ions in a rural area impacted by biomass burning emissions, Atmospheric environment, 45, 5260-5265, https://doi.org/10.1016/j.atmosenv.2011.06.063, 2011.

Compernolle, S. and Müller, J. F.: Henry's law constants of diacids and hydroxy polyacids: recommended values, Atmos. Chem. Phys., 14, 2699-2712, https://doi.org/10.5194/acp-14-2699-2014, 2014.

Davey, M. E. and O'toole, G. A.: Microbial biofilms: from ecology to molecular genetics, Microbiology and molecular biology reviews, 64, 847-867, https://doi.org/10.1128/MMBR.64.4.847-867.2000, 2000.

Delort, A.-M., Vaïtilingom, M., Amato, P., Sancelme, M., Parazols, M., Mailhot, G., Laj, P., and Deguillaume, L.: A short overview of the microbial population in clouds: Potential roles in atmospheric chemistry and nucleation processes, Atmospheric Research, 98, 249-260, 10.1016/j.atmosres.2010.07.004, 2010.

Després, V., Huffman, J. A., Burrows, S. M., Hoose, C., Safatov, A., Buryak, G., Fröhlich-Nowoisky, J., Elbert, W., Andreae, M., Pöschl, U., and Jaenicke, R.: Primary biological aerosol particles in the atmosphere: a review, Tellus B: Chemical and Physical Meteorology, 64, https://doi.org/10.3402/tellusb.v64i0.15598, 2012.

Ding, W., Li, L., Han, Y., Liu, J., and Liu, J.: Site-related and seasonal variation of bioaerosol emission in an indoor wastewater treatment station: level, characteristics of particle size, and microbial structure, Aerobiologia, 32, 211-224, https://doi.org/10.1007/s10453-015-9391-5, 2015.

Ervens, B. and Amato, P.: The global impact of bacterial processes on carbon mass, Atmospheric Chemistry and Physics, 20, 1777-1794, https://doi.org/10.5194/acp-20-1777-2020, 2020.

Ervens, B., Gligorovski, S., and Herrmann, H.: Temperature-dependent rate constants for hydroxyl radical reactions with organic compounds in aqueous solutions, Physical Chemistry Chemical Physics, 5, 1811-1824, https://doi.org/10.1039/B300072A, 2003.

Ervens, B., Turpin, B. J., and Weber, R. J.: Secondary organic aerosol formation in cloud droplets and aqueous particles (aqSOA): a review of laboratory, field and model studies, Atmos. Chem. Phys., 11, 11069-11102, 10.5194/acp-11-11069-2011, 2011.

Fankhauser, A. M., Antonio, D. D., Krell, A., Alston, S. J., Banta, S., and McNeill, V. F.: Constraining the Impact of Bacteria on the Aqueous Atmospheric Chemistry of Small Organic Compounds, ACS Earth and Space Chemistry, 3, 1485-1491, 10.1021/acsearthspacechem.9b00054, 2019.

Flemming, H. C. and Wingender, J.: The biofilm matrix, Nature Reviews Microbiology, 8, 623-633, https://doi.org/10.1038/nrmicro2415, 2010.

George, K. M., Ruthenburg, T. C., Smith, J., Yu, L., Zhang, Q., Anastasio, C., and Dillner, A. M.: FT-IR quantification of the carbonyl functional group in aqueous-phase secondary organic aerosol from phenols, Atmospheric Environment, 100, 230-237, https://doi.org/10.1016/j.atmosenv.2014.11.011, 2015.

Gioda, A., Reyes-Rodriguez, G. J., Santos-Figueroa, G., Collett, J. L., Decesari, S., Ramos, M., Netto, H., Neto, F. R. D., and Mayol-Bracero, O. L.: Speciation of water-soluble inorganic, organic, and total nitrogen in a background marine environment: Cloud water, rainwater, and aerosol particles, Journal of Geophysical Research-Atmospheres, 116, https://doi.org/10.1029/2010jd015010, 2011.

Gowda, H., Ivanisevic, J., Johnson, C. H., Kurczy, M. E., Benton, H. P., Rinehart, D., Nguyen, T., Ray, J., Kuehl, J., Arevalo, B., Westenskow, P. D., Wang, J., Arkin, A. P., Deutschbauer, A. M., Patti, G. J., and Siuzdak, G.: Interactive XCMS Online: simplifying advanced metabolomic data processing and subsequent statistical analyses, Anal Chem, 86, 6931-6939, https://doi.org/10.1021/ac500734c, 2014.

Guan, N. and Liu, L.: Microbial response to acid stress: mechanisms and applications, Applied Microbiology and Biotechnology, 104, 51-65, https://doi.org/10.1007/s00253-019-10226-1, 2020.

Guo, H., Liu, J., Froyd, K. D., Roberts, J. M., Veres, P. R., Hayes, P. L., Jimenez, J. L., Nenes, A., and Weber, R. J.: Fine particle pH and gas–particle phase partitioning of inorganic species in Pasadena, California, during the 2010 CalNex campaign, Atmos. Chem. Phys., 17, 5703-5719, https://doi.org/10.5194/acp-17-5703-2017, 2017.

Guo, H., Sullivan, A. P., Campuzano-Jost, P., Schroder, J. C., Lopez-Hilfiker, F. D., Dibb, J. E., Jimenez, J. L., Thornton, J. A., Brown, S. S., Nenes, A., and Weber, R. J.: Fine particle pH and the partitioning of nitric acid during winter in the northeastern United States, Journal of Geophysical Research: Atmospheres, 121, 10,355-310,376, https://doi.org/10.1002/2016JD025311, 2016.

Haynes, W. M.: CRC handbook of chemistry and physics, CRC Press, Boca Raton, Florida2014.

Herrmann, H., Hoffmann, D., Schaefer, T., Brauer, P., and Tilgner, A.: Tropospheric aqueous-phase free-radical chemistry: radical sources, spectra, reaction kinetics and prediction tools, Chemphyschem, 11, 3796-3822, https://doi.org/10.1002/cphc.201000533, 2010.

Hu, W., Niu, H. Y., Murata, K., Wu, Z. J., Hu, M., Kojima, T., and Zhang, D. Z.: Bacteria in atmospheric waters: Detection, characteristics and implications, Atmospheric Environment, 179, 201-221, https://doi.org/10.1016/j.atmosenv.2018.02.026, 2018.

Huang, D. D., Zhang, Q., Cheung, H. H. Y., Yu, L., Zhou, S., Anastasio, C., Smith, J. D., and Chan, C. K.: Formation and Evolution of aqSOA from Aqueous-Phase Reactions of Phenolic Carbonyls: Comparison between Ammonium Sulfate and Ammonium Nitrate Solutions, Environmental Science & Technology, 52, 9215-9224, https://doi.org/10.1021/acs.est.8b03441, 2018.

Huang, S., Hu, W., Chen, J., Wu, Z., Zhang, D., and Fu, P.: Overview of biological ice nucleating particles in the atmosphere, Environment International, 146, 106197, https://doi.org/10.1016/j.envint.2020.106197, 2021.

Huang, X.-F., Li, X., He, L.-Y., Feng, N., Hu, M., Niu, Y.-W., and Zeng, L.-W.: 5-Year study of rainwater chemistry in a coastal mega-city in South China, Atmospheric Research, 97, 185-193, https://doi.org/10.1016/j.atmosres.2010.03.027, 2010.

Husárová, S., Vaïtilingom, M., Deguillaume, L., Traikia, M., Vinatier, V., Sancelme, M., Amato, P., Matulová, M., and Delort, A.-M.: Biotransformation of methanol and formaldehyde by bacteria isolated from clouds. Comparison with radical chemistry, Atmospheric Environment, 45, 6093-6102, 10.1016/j.atmosenv.2011.06.035, 2011.

Jaber, S., Joly, M., Brissy, M., Leremboure, M., Khaled, A., Ervens, B., and Delort, A.-M.: Biotic and abiotic transformation of amino acids in cloud water: experimental studies and atmospheric implications, Biogeosciences, 18, 1067-1080, 10.5194/bg-18-1067-2021, 2021.

Jaber, S., Lallement, A., Sancelme, M., Leremboure, M., Mailhot, G., Ervens, B., and Delort, A.-M.: Biodegradation of phenol and catechol in cloud water: comparison to chemical oxidation in the atmospheric multiphase system, Atmospheric Chemistry and Physics, 20, 4987-4997, 10.5194/acp-20-4987-2020, 2020.

Jaenicke, R.: Abundance of cellular material and proteins in the atmosphere, Science, 308, 73-73, https://doi.org/10.1126/science.1106335, 2005.

Jain, C., Rodriguez-R, L. M., Phillippy, A. M., Konstantinidis, K. T., and Aluru, S.: High throughput ANI analysis of 90K prokaryotic genomes reveals clear species boundaries, Nature communications, 9, 1-8, https://doi.org/10.1038/s41467-018-07641-9, 2018.

Joly, M., Amato, P., Sancelme, M., Vinatier, V., Abrantes, M., Deguillaume, L., and Delort, A.-M.: Survival of microbial isolates from clouds toward simulated atmospheric stress factors, Atmospheric Environment, 117, 92-98, https://doi.org/10.1016/j.atmosenv.2015.07.009, 2015.

Kanehisa, M., Sato, Y., and Kawashima, M.: KEGG mapping tools for uncovering hidden features in biological data, Protein Science, 31, 47-53, https://doi.org/10.1002/pro.4172, 2022.

Koutny, M., Sancelme, M., Dabin, C., Pichon, N., Delort, A.-M., and Lemaire, J.: Acquired biodegradability of polyethylenes containing pro-oxidant additives, Polymer Degradation and Stability, 91, 1495-1503, 10.1016/j.polymdegradstab.2005.10.007, 2006.

Laszakovits, J. R. and MacKay, A. A.: Data-Based Chemical Class Regions for Van Krevelen Diagrams, Journal of the American Society for Mass Spectrometry, 33, 198-202, https://doi.org/10.1021/jasms.1c00230, 2022.

Li, T., Wang, Z., Wang, Y., Wu, C., Liang, Y., Xia, M., Yu, C., Yun, H., Wang, W., Wang, Y., Guo, J., Herrmann, H., and Wang, T.: Chemical characteristics of cloud water and the impacts on aerosol properties at a subtropical mountain site in Hong Kong SAR, Atmospheric Chemistry and Physics, 20, 391-407, https://doi.org/10.5194/acp-20-391-2020, 2020.

Lide, D. R. and Frederikse, H. P. R.: CRC handbook of chemistry and physics, Boca Raton, Florida1995.

Löflund, M., Kasper-Giebl, A., Schuster, B., Giebl, H., Hitzenberger, R., and Puxbaum, H.: Formic, acetic, oxalic, malonic and succinic acid concentrations and their contribution to organic carbon in cloud water, Atmospheric Environment, 36, 1553-1558, https://doi.org/10.1016/S1352-2310(01)00573-8, 2002.

Lund, P., Tramonti, A., and De Biase, D.: Coping with low pH: molecular strategies in neutralophilic bacteria, FEMS Microbiology Reviews, 38, 1091-1125, https://doi.org/10.1111/1574-6976.12076, 2014.

Makuc, J., Paiva, S., Schauen, M., Krämer, R., André, B., Casal, M., Leão, C., and Boles, E.: The putative monocarboxylate permeases of the yeast Saccharomyces cerevisiae do not transport monocarboxylic acids across the plasma membrane, Yeast, 18, 1131-1143, 2001.

Manni, M., Berkeley, M. R., Seppey, M., and Zdobnov, E. M.: BUSCO: assessing genomic data quality and beyond, Current Protocols, 1, e323, https://doi.org/10.1002/cpz1.323, 2021.

Matulova, M., Husarova, S., Capek, P., Sancelme, M., and Delort, A. M.: Biotransformation of various saccharides and production of exopolymeric substances by cloud-borne Bacillus sp. 3B6, Environ Sci Technol, 48, 14238-14247, 10.1021/es501350s, 2014.

Meier-Kolthoff, J. P. and Göker, M.: TYGS is an automated high-throughput platform for state-of-the-art genome-based taxonomy, Nature communications, 10, 1-10, https://doi.org/10.1038/s41467-019-10210-3, 2019.

Meskhidze, N., Chameides, W. L., Nenes, A., and Chen, G.: Iron mobilization in mineral dust: Can anthropogenic SO2 emissions affect ocean productivity?, Geophysical Research Letters, 30, https://doi.org/10.1029/2003GL018035, 2003.

Misovich, M. V., Hettiyadura, A. P. S., Jiang, W. Q., Zhang, Q., and Laskin, A.: Molecular-Level Study of the Photo-Oxidation of Aqueous-Phase Guaiacyl Acetone in the Presence of C-3*: Formation of Brown Carbon Products, Acs Earth and Space Chemistry, 5, 1983-1996, https://doi.org/10.1021/acsearthspacechem.1c00103, 2021.

Möhler, O., DeMott, P., Vali, G., and Levin, Z.: Microbiology and atmospheric processes: the role of biological particles in cloud physics, Biogeosciences, 4, 1059-1071, https://doi.org/10.5194/bg-4-1059-2007, 2007.

Morris, C. E., Soubeyrand, S., Bigg, E. K., Creamean, J. M., and Sands, D. C.: Mapping Rainfall Feedback to Reveal the Potential Sensitivity of Precipitation to Biological Aerosols, Bulletin of the American Meteorological Society, 98, 1109-1118, https://doi.org/10.1175/BAMS-D-15-00293.1, 2017.

Morris, C. E., Conen, F., Alex Huffman, J., Phillips, V., Pöschl, U., and Sands, D. C.: Bioprecipitation: a feedback cycle linking earth history, ecosystem dynamics and land use through biological ice nucleators in the atmosphere, Glob Chang Biol, 20, 341-351, https://doi.org/10.1111/gcb.12447, 2014.

526 Nah, T., Guo, H., Sullivan, A. P., Chen, Y., Tanner, D. J., Nenes, A., Russell, A., Ng, N. L.,
527 Huey, L. G., and Weber, R. J.: Characterization of aerosol composition, aerosol acidity, and
528 organic acid partitioning at an agriculturally intensive rural southeastern US site, Atmos. Chem.
529 Phys., 18, 11471-11491, https://doi.org/10.5194/acp-18-11471-2018, 2018.

530 Pang, Z., Chong, J., Zhou, G., de Lima Morais, D. A., Chang, L., Barrette, M., Gauthier, C.,
531 Jacques, P. E., Li, S., and Xia, J.: MetaboAnalyst 5.0: narrowing the gap between raw spectra
532 and functional insights, Nucleic Acids Res, 49, W388-W396,
533 https://doi.org/10.1093/nar/gkab382, 2021.

534 Peng, J., Zhou, S., Xiao, K., Zeng, J., Yao, C., Lu, S., Zhang, W., Fu, Y., Yang, Y., and Bi, X.:
535 Diversity of bacteria in cloud water collected at a National Atmospheric Monitoring Station in
536 Southern China, Atmospheric Research, 218, 176-182,
537 https://doi.org/10.1016/j.atmosres.2018.12.004, 2019.

538 Prokof'eva, T. V., Shoba, S. A., Lysak, L. V., Ivanova, A. E., Glushakova, A. M., Shishkov, V.
539 A., Lapygina, E. V., Shilaika, P. D., and Glebova, A. A.: Organic Constituents and Biota in the
540 Urban Atmospheric Solid Aerosol: Potential Effects on Urban Soils, Eurasian Soil Science, 54,
541 1532-1545, https://doi.org/10.1134/S1064229321100094, 2021.

542 Pye, H. O., Nenes, A., Alexander, B., Ault, A. P., Barth, M. C., Clegg, S. L., Collett Jr, J. L.,
543 Fahey, K. M., Hennigan, C. J., and Herrmann, H.: The acidity of atmospheric particles and
544 clouds, Atmospheric chemistry and physics, 20, 4809-4888, https://doi.org/10.5194/acp-20-
545 4809-2020, 2020.

546 Qu, R. and Han, G.: A critical review of the variation in rainwater acidity in 24 Chinese cities
547 during 1982–2018, Elementa: Science of the Anthropocene, 9,
548 https://doi.org/10.1525/elementa.2021.00142, 2021.

549 Rivas-Ubach, A., Liu, Y., Bianchi, T. S., Tolic, N., Jansson, C., and Pasa-Tolic, L.: Moving
550 beyond the van Krevelen diagram: A new stoichiometric approach for compound classification
551 in organisms, Analytical chemistry, 90, 6152-6160, 2018.

552 Romano, S., Fragola, M., Alifano, P., Perrone, M. R., and Talà, A.: Potential Human and Plant
553 Pathogenic Species in Airborne PM10 Samples and Relationships with Chemical Components
554 and Meteorological Parameters, Atmosphere, 12, 654, https://doi.org/10.3390/atmos12050654,
555 2021.

556 Romano, S., Di Salvo, M., Rispoli, G., Alifano, P., Perrone, M. R., and Tala, A.: Airborne
557 bacteria in the Central Mediterranean: Structure and role of meteorology and air mass transport,
558 Sci Total Environ, 697, 134020, https://doi.org/10.1016/j.scitotenv.2019.134020, 2019.

559 Ruiz-Gil, T., Acuña, J. J., Fujiyoshi, S., Tanaka, D., Noda, J., Maruyama, F., and Jorquera, M.
560 A.: Airborne bacterial communities of outdoor environments and their associated influencing
561 factors, Environment International, 145, 106156, https://doi.org/10.1016/j.envint.2020.106156,
562 2020.

563 Sander, R.: Compilation of Henry's law constants (version 4.0) for water as solvent, Atmos.
564 Chem. Phys., 15, 4399-4981, https://doi.org/10.5194/acp-15-4399-2015, 2015.

565 Saxena, P. and Hildemann, L. M.: Water-soluble organics in atmospheric particles: A critical
566 review of the literature and application of thermodynamics to identify candidate compounds,
567 Journal of Atmospheric Chemistry, 24, 57-109, https://doi.org/10.1007/BF00053823, 1996.

568 Seemann, T.: Prokka: rapid prokaryotic genome annotation, Bioinformatics, 30, 2068-2069,
569 https://doi.org/10.1093/bioinformatics/btu153, 2014.

570 Shah, V., Jacob, D. J., Moch, J. M., Wang, X., and Zhai, S.: Global modeling of cloud water
571 acidity, precipitation acidity, and acid inputs to ecosystems, Atmos. Chem. Phys., 20, 12223-
572 12245, https://doi.org/10.5194/acp-20-12223-2020, 2020.

573 Song, F. and Gao, Y.: Chemical characteristics of precipitation at metropolitan Newark in the
574 US East Coast, Atmospheric Environment, 43, 4903-4913,
575 https://doi.org/10.1016/j.atmosenv.2009.07.024, 2009.

576 Sun, X., Wang, Y., Li, H., Yang, X., Sun, L., Wang, X., Wang, T., and Wang, W.: Organic acids
577 in cloud water and rainwater at a mountain site in acid rain areas of South China, Environ Sci
578 Pollut Res Int, 23, 9529-9539, 10.1007/s11356-016-6038-1, 2016.

579 Sündermann, A., Eggers, L. F., and Schwudke, D.: Liquid Extraction: Bligh and Dyer, in:
580 Encyclopedia of Lipidomics, 1-4, https://doi.org/10.1007/978-94-007-7864-1_88-1, 2016.

581 Tilgner, A., Schaefer, T., Alexander, B., Barth, M., Collett Jr, J. L., Fahey, K. M., Nenes, A.,
582 Pye, H. O., Herrmann, H., and McNeill, V. F.: Acidity and the multiphase chemistry of
583 atmospheric aqueous particles and clouds, Atmospheric Chemistry and Physics, 21, 13483-
584 13536, 2021.

585 Tsai, Y. I. and Kuo, S.-C.: Contributions of low molecular weight carboxylic acids to aerosols
586 and wet deposition in a natural subtropical broad-leaved forest environment, Atmospheric
587 Environment, 81, 270-279, https://doi.org/10.1016/j.atmosenv.2013.08.061, 2013.

588 Tyagi, P., Ishimura, Y., and Kawamura, K.: Hydroxy fatty acids in marine aerosols as microbial
589 tracers: 4-year study on β-and ω-hydroxy fatty acids from remote Chichijima Island in the
590 western North Pacific, Atmospheric Environment, 115, 89-100, 2015.

591 Vaitilingom, M., Amato, P., Sancelme, M., Laj, P., Leriche, M., and Delort, A. M.: Contribution
592 of microbial activity to carbon chemistry in clouds, Appl Environ Microbiol, 76, 23-29,
593 10.1128/AEM.01127-09, 2010.

594 Vaitilingom, M., Deguillaume, L., Vinatier, V., Sancelme, M., Amato, P., Chaumerliac, N., and
595 Delort, A. M.: Potential impact of microbial activity on the oxidant capacity and organic carbon
596 budget in clouds, Proc Natl Acad Sci U S A, 110, 559-564, 10.1073/pnas.1205743110, 2013.

597 Vaïtilingom, M., Attard, E., Gaiani, N., Sancelme, M., Deguillaume, L., Flossmann, A. I.,

598 Amato, P., and Delort, A.-M.: Long-term features of cloud microbiology at the puy de Dôme
599 (France), Atmospheric Environment, 56, 88-100,
600 https://doi.org/10.1016/j.atmosenv.2012.03.072, 2012.

601 Vaïtilingom, M., Charbouillot, T., Deguillaume, L., Maisonobe, R., Parazols, M., Amato, P.,
602 Sancelme, M., and Delort, A. M.: Atmospheric chemistry of carboxylic acids: microbial
603 implication versus photochemistry, Atmospheric Chemistry and Physics, 11, 8721-8733,
604 10.5194/acp-11-8721-2011, 2011.

605 Watson, J., Baker, T., and Bell, S.: Molecular biology of the gene, 6th edn. W, 2007.

606 Weast, R. C. and Astle, M. J.: CRC Handbook of Chemistry and Physics, CRC Press1981.

607 Wei, M., Xu, C., Chen, J., Zhu, C., Li, J., and Lv, G.: Characteristics of bacterial community in
608 cloud water at Mt Tai: similarity and disparity under polluted and non-polluted cloud episodes,
609 Atmos. Chem. Phys., 17, 5253-5270, https://doi.org/10.5194/acp-17-5253-2017, 2017.

610 pKa data compiled by R. Williams:
611 https://organicchemistrydata.org/hansreich/resources/pka/pka_data/pka-compilation-
612 williams.pdf, last access: 7 Dec 2022.

613 Xu, G., Lee, X., and Lv, Y.: Urban and rural observations of carboxylic acids in rainwater in
614 Southwest of China: the impact of urbanization, Journal of atmospheric chemistry, 62, 249-
615 260, https://doi.org/10.1007/s10874-010-9151-4, 2009.

616 Zhang, M., Khaled, A., Amato, P., Delort, A. M., and Ervens, B.: Sensitivities to biological
617 aerosol particle properties and ageing processes: potential implications for aerosol–cloud
618 interactions and optical properties, Atmos. Chem. Phys., 21, 3699-3724,
619 https://doi.org/10.5194/acp-21-3699-2021, 2021.

620 Zhang, Y., Lee, X., and Cao, F.: Chemical characteristics and sources of organic acids in
621 precipitation at a semi-urban site in Southwest China, Atmospheric environment, 45, 413-419,
622 https://doi.org/10.1016/j.atmosenv.2010.09.067, 2011.

623 Zhao, W., Wang, Z., Li, S., Li, L., Wei, L., Xie, Q., Yue, S., Li, T., Liang, Y., and Sun, Y.: Water-
624 soluble low molecular weight organics in cloud water at Mt. Tai Mo Shan, Hong Kong, Science
625 of the Total Environment, 697, 134095, https://doi.org/10.1016/j.scitotenv.2019.134095, 2019.

626 Zhou, H., Wang, X., Li, Z., Kuang, Y., Mao, D., and Luo, Y.: Occurrence and Distribution of
627 Urban Dust-Associated Bacterial Antibiotic Resistance in Northern China, Environmental
628 Science & Technology Letters, 5, 50-55, https://doi.org/10.1021/acs.estlett.7b00571, 2018.

629 Zhu, C., Chen, J., Wang, X., Li, J., Wei, M., Xu, C., Xu, X., Ding, A., and Collett, J. L.:
630 Chemical Composition and Bacterial Community in Size-Resolved Cloud Water at the Summit
631 of Mt. Tai, China, Aerosol and Air Quality Research, 18, 1-14,
632 https://doi.org/10.4209/aaqr.2016.11.0493, 2018.
633